PERGAMON

Deep-Sea Research II 48 (2001) 1609–1648

DEEP-SEA RESEARCH
PART II

www.elsevier.com/locate/dsr2

Modeling the effect of nitrogen fixation on carbon and nitrogen fluxes at BATS

Raleigh R. Hood[a,*], Nicholas R. Bates[b], Douglas G. Capone[a,1], Donald B. Olson[c]

[a]*Center for Environmental Science, Horn Point Laboratory, University of Maryland, Cambridge, MD 21613-0775, USA*
[b]*Bermuda Biological Station for Research, Inc., GE01, Bermuda*
[c]*Rosenstiel School of Marine and Atmospheric Science, University of Miami, Miami, FL 33149, USA*

Abstract

Recent geochemical estimates of N_2-fixation in the North Atlantic ocean indicate rates that are significantly higher than those derived from direct observations. In this paper different N_2-fixation rate scenarios are explored using a one-dimensional, biogeochemical model that includes an explicit representation of *Trichodesmium*. This model reproduces most of the observed interannual variability in phytoplankton production and generates seasonal *Trichodesmium* biomass and N_2-fixation cycles similar to those observed at BATS. Two solutions are presented, one where the N_2-fixation rate is increased enough to reproduce the observed summertime drawdown of DIC, and a second where it is tuned to reproduce the observed sediment trap fluxes. The high N_2-fixation solution reproduces the seasonal and interannual variability in DIC concentrations quite accurately and generates N_2-fixation rates that agree with direct rate measurements from 1990 and recent geochemical estimates. However, this solution generates export fluxes that are more than 4 times higher than those observed, and predicts the development of DON and DOC anomalies in late summer/early fall that have not been observed. In contrast, the low N_2-fixation solution generates trap fluxes that are approximately correct, but overestimates the summertime DIC concentrations by 20–30 $\mu mol/kg^{-1}$. Both solutions indicate that there is significant interannual variability in N_2-fixation at BATS and that the rates were much lower in 1995–1996 than in the previous six years. It is suggested that this variability is linked to decadal-scale fluctuations in the North Atlantic climate.

1. Introduction

Efforts to simulate biogeochemical processes in the oceans have increased tremendously in the last decade, largely in response to concerns about increasing atmospheric CO_2 concentrations and

* Corresponding author. Tel.: + 1-4102288200; fax: + 1-4102218490.
E-mail address: raleigh@hpl.umces.edu (R.R. Hood).
[1] Now at Wrigley Institute, University of Southern California, LA 90089, USA.

0967-0645/01/$ - see front matter
PII: S0967-0645(00)00160-0

the need to understand the oceans role in cycling and sequestering anthropogenic CO_2. In spite of this growth, there are still significant gaps in our knowledge and many problems that remain to be solved. One outstanding question is the significance of the role of N_2-fixation in the global carbon cycle. N_2-fixation may be important because primary production supported by it can result in a net export of carbon from the surface waters and a net drawdown of atmospheric carbon dioxide, and because the global balance between N_2-fixation and denitrification determines the degree to which the oceans are nitrogen (N) limited (Codispoti, 1989; Falkowski, 1997). Although early estimates suggested that N_2-fixation is not a significant source of "new" N (Capone and Carpenter, 1982), more recent estimates indicate that the input of reactive N from the atmosphere to the oceans due to N_2-fixation can be comparable to the nitrate-based upwelling flux in oligotrophic tropical waters (Karl et al., 1997; Capone et al., 1997), and recent geochemical studies suggest that the rates are even higher (Michaels et al., 1996; Gruber and Sarmiento, 1997).

Discrepancies between different N_2-fixation rate estimates have been the subject of recent debate (Michaels and Knap, 1996; Michaels et al., 1996; Lipschultz and Owens, 1996; Gruber and Sarmiento, 1997; Capone et al., 1997; Orcutt et al., 2001; Hood et al., 2000). Current estimates of the global N_2-fixation rate range from 10 to 200 Tg N yr^{-1}, with the direct rate estimates tending toward the low end of this range (e.g., Carpenter and Capone, 1992) and indirect geochemically based estimates tending toward the higher end of this range (e.g., Michaels et al., 1996; Gruber and Sarmiento, 1997). In the North Atlantic ocean, which is the region considered in this paper, N_2-fixation rate estimates span a similarly large range. For example, recent geochemical estimates of N_2-fixation based upon observed excess NO_3 relative to phosphorus in the thermocline in the Sargasso Sea suggest that the rates may be as high as 230 mmol N m^{-2} yr^{-1} (Michaels et al., 1996). In contrast, earlier direct measurements in the Sargasso Sea based upon the acetylene reduction technique suggest annual rates that are two orders of magnitude lower (Carpenter and McCarthy, 1975; Carpenter and Price, 1977).

Although most of the direct measurements cannot be reconciled with the high geochemical estimates, there is other geochemical evidence that corroborates them. Measurements of dissolved inorganic carbon (DIC) concentrations at the Bermuda Atlantic Time-Series (BATS) station have revealed consistent depletions of carbon from surface waters during late summer and early fall (Michaels et al., 1994; Bates et al., 1996). Presumably this is due to the uptake of inorganic carbon by phytoplankton, but there does not appear to be any excess reactive nitrogen in the surface waters to support it. One explanation, consistent with the geochemical estimates, is that the nitrogen that supports the drawdown is derived from the atmosphere through N_2-fixation (Michaels et al., 1996). This explanation is supported by $\delta\ ^{13}C$ data reported by Gruber et al. (1998), which indicates that the DIC drawdown is due to primary production. In addition, $\delta\ ^{15}N$ measurements have revealed anomalously low values in particulate matter and zooplankton in surface waters, and nitrate in the nitracline in the subtropical North Atlantic, suggesting a significant atmospheric N source (Altabet, 1988; Carpenter and Capone, 1997; Montoya et al., submitted). And there is one set of direct rate estimates that are consistent with the high geochemical rates: Carpenter and Romans (1991) measured *Trichodesmium* colony concentrations in the Western Sargasso Sea ranging from 1000 to 2000 colonies m^{-3}, which suggests daily rates of 0.7–1.4 mmol N m^{-2} d^{-1} (assuming a 50 m deep water column, but see also Lipschultz and Owens, 1996) and annual rates of 128–256 mmol N m^{-2} yr^{-1} (assuming a six-month growing season).

In this paper we describe solutions from a one-dimensional, biogeochemical model that was specifically designed to explore the effects of different levels of N_2-fixation on C and N fluxes in the Sargasso Sea. This model is an N-based ecosystem model that includes a carbon system sub-model and an explicit dynamic representations of dissolved organic nitrogen (DON) and N_2-fixation by the diazotrophic cyanobacterium *Trichodesmium*. Although quite simple, this system reproduces the observed seasonal and interannual variability in phytoplankton production quite well and generates seasonal *Trichodesmium* biomass and N_2-fixation rate cycles similar to those observed at BATS (Orcutt et al., 2001). Two solutions are presented, one where the N_2-fixation rate is increased enough to reproduce the observed summertime drawdown of DIC, and another tuned to reproduce the observed sediment trap fluxes.

2. The model

The three basic components of the coupled system include: (1) a six-compartment ecosystem model specifically designed for simulating nitrogen cycling at BATS; (2) a thermodynamic CO_2 chemistry model that accounts for the effects of variations in DIC, alkalinity, temperature and pressure on pCO_2 and air–sea CO_2 exchange; and (3) a modified version of the Price et al. (1986) mixed-layer model that simulates vertical mixing using atmospheric forcing data from Bermuda. In addition, in this section the data used to parameterize, initialize, force and restore the model are discussed.

The source code for this model is available upon request from lead author (R. Hood).

2.1. The ecosystem model

The six-compartment ecosystem model includes state variables representing dissolved inorganic nitrogen (DIN), dissolved organic nitrogen (DON), phytoplankton (P), *Trichodesmium* (T), detritus (D) and heterotrophs (H) (Fig. 1). The mass in each of these compartments is expressed in nitrogen concentration units (mmol $N\,m^{-3}$), and the model parameters are listed in Table 1.

The H compartment is considered to represent the sum of all heterotrophic processes including, for example, bacteria, microzooplankton and mesozooplankton. Changes in H due to biological processes are determined as follows:

$$\frac{\partial H}{\partial t} = \mathrm{ge}_P\, h_P H C_\mathrm{m} P + \mathrm{ge}_D\, h_D H C_\mathrm{m} D + (\mathrm{ge}_H - 1) h_H C_\mathrm{m} H^2 + \mathrm{ge}_T\, h_T H C_\mathrm{m} T + \mathrm{ge}_\mathrm{DON}\, h_\mathrm{DON} H C_\mathrm{m}\,\mathrm{DON}, \quad (1)$$

where the coefficients ge_i are heterotrophic growth efficiencies, for growth on phytoplankton ($i = P$), *Trichodesmium* ($i = T$), detritus ($i = D$), DON ($i = \mathrm{DON}$) and other heterotrophs ($i = H$). The coefficient C_m is the maximum heterotrophic consumption rate. In (1)

$$h_P = \Phi_P/\Theta, \quad (2)$$

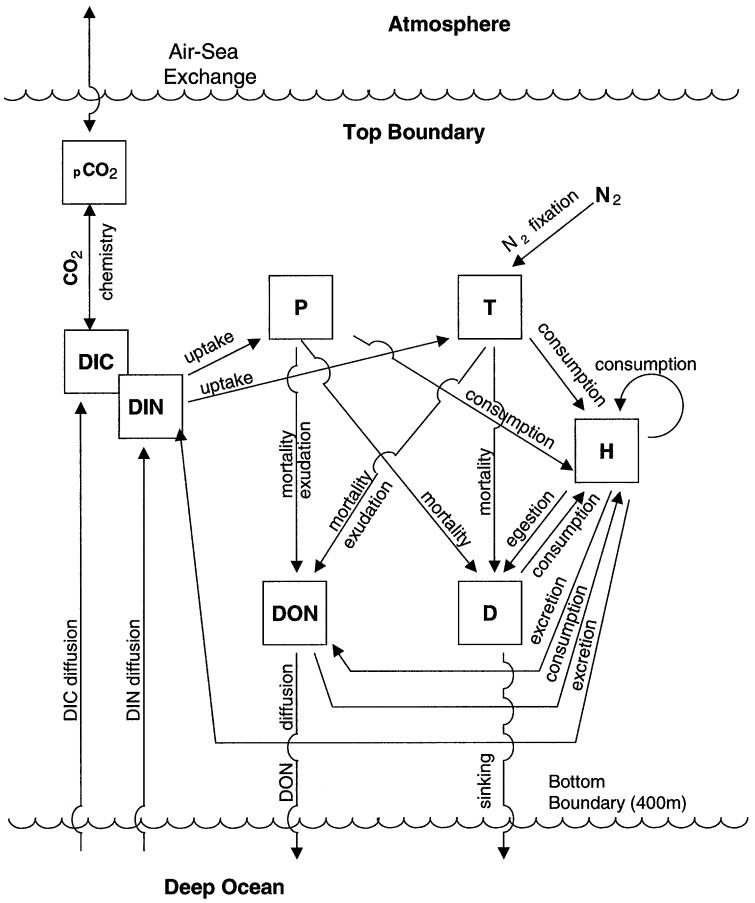

Fig. 1. A schematic box diagram of the ecosystem model showing the relationship to the CO_2 chemistry model and the pathways for air–sea and deep-ocean nitrogen and carbon exchange. The state variables in the ecosystem model are dissolved inorganic nitrogen (DIN), dissolved organic nitrogen (DON), phytoplankton (P), *Trichodesmium* (T), heterotrophs (H) and detritus (D). In the carbon system only one explicit state variable is represented, dissolved inorganic carbon (DIC).

$$h_D = \Phi_D/\Theta, \tag{3}$$

$$h_H = \Phi_H/\Theta, \tag{4}$$

$$h_T = \Phi_T/\Theta, \tag{5}$$

$$h_{\mathrm{DON}} = \Phi_{\mathrm{DON}}/\Theta \tag{6}$$

and

$$\Theta = \Phi_P P + \Phi_D D + \Phi_H H + \Phi_T T + \Phi_{\mathrm{DON}}\,\mathrm{DON} + \mathrm{HKS}, \tag{7}$$

Table 1
Model parameter symbols, units and values used in the mainrun solutions

Description	Symbol	Value	Units
Biological parameters			
Growth efficiency for H on P	ge_P	0.20	Dimensionless
Growth efficiency for H on T	ge_T	0.20	Dimensionless
Growth efficiency for H on DON	ge_{DON}	0.20	Dimensionless
Growth efficiency for H on D	ge_D	0.20	Dimensionless
Growth efficiency for H on H	ge_H	0.20	Dimensionless
Assimilation efficiency for H on P	ae_P	0.70	Dimensionless
Assimilation efficiency for H on T	ae_T	0.70	Dimensionless
Assimilation efficiency for H on DON	ae_{DON}	1.0	Dimensionless
Assimilation efficiency for H on D	ae_D	0.70	Dimensionless
Assimilation efficiency for H on H	ae_H	0.70	Dimensionless
Partitioning of P and T senesence	β	0.25	Dimensionless
Partitioning of P and T production	α	0.70	Dimensionless
Partitioning of excretion to DIN	γ	0.75	Dimensionless
Maximum phytoplankton growth rate	μ_P	3.22	d^{-1}
Maximum *Trichodesmium* growth rate	μ_T	0.17	d^{-1}
Phytoplankton light saturation parameter	I_P	40.0	W m^{-2}
Phytoplankton photoinhibition parameter	$I_{\beta P}$	400.0	W m^{-2}
Trichodesmium light saturation parameter	I_T	80.0	W m^{-2}
Trichodesmium light saturation parameter	$I_{\beta T}$	0	W m^{-2}
Sat. const. for DIN uptake by P	PK_s	0.5	mmol m^{-3}
Sat. const. for DIN uptake by T	TK_s	0.5	mmol m^{-3}
Phytoplankton natural mortality rate	S_P	0.01	d^{-1}
Trichodesmium natural mortality rate	S_T	0.021, 0.0235	d^{-1}
Heterotropic maximum consumption rate	C_m	6.4	d^{-1}
Sat. const. for heterotropic consumption	HK_s	0.80	mmol m^{-3}
Heterotropic preference for P	Φ_P	1/4	Dimensionless
Heterotropic preference for D	Φ_D	1/4	Dimensionless
Heterotropic preference for H	Φ_H	1/4	Dimensionless
Heterotropic preference for T	Φ_T	0	Dimensionless
Heterotropic preference for DON	Φ_{DON}	1/4	Dimensionless
Phytoplankton-specific attenuation coeff.	k_p	0.0223	m^2 $mmol^{-1}$ N
Detritus sinking rate	w	12,4	m d^{-1}
Physical parameters			
Vertical resolution	ΔZ	1.0	m
Time step	Δt	3600	s
Diffusion coefficient	K_w	0.0001	m^2 s^{-1}
Shortwave extinction coefficient	k_x	0.03	m^{-1}
Temperature restoration time scale	T_T	41.66	d
Salinity restoration time scale	T_S	41.66	d

which allows assignment of "preferences" for the different forms of organic nitrogen (cf., Fasham et al., 1990; McCreary et al., 1996). For simplicity, the half-saturation constant, HKS, is assumed to be the same for all substrates.

The DIN compartment is considered to represent the sum of all dissolved inorganic forms of nitrogen, i.e., NO_3, NO_2 and NH_4^+. Changes in DIN, due to biological processes are determined as follows:

$$\frac{\partial \mathrm{DIN}}{\partial t} = \gamma(\mathrm{ae}_P - \mathrm{ge}_P)h_P HC_\mathrm{m} P + \gamma(\mathrm{ae}_D - \mathrm{ge}_D)h_D HC_\mathrm{m} D + \gamma(\mathrm{ae}_H - \mathrm{ge}_H)h_H HC_\mathrm{m} H + \gamma(\mathrm{ae}_T - \mathrm{ge}_T)h_T HC_\mathrm{m} T + (\mathrm{ae}_\mathrm{DON} - \mathrm{ge}_\mathrm{DON})h_\mathrm{DON} HC_\mathrm{m}\,\mathrm{DON} - U_P P - U_T T, \quad (8)$$

where the positive terms represent heterotrophic remineralization of particulate and dissolved organic nitrogen to dissolved inorganic nitrogen, and the negative terms represent uptake of DIN by phytoplankton and *Trichodesmium*. The coefficients ae_i are assimilation efficiencies for heterotrophic growth on phytoplankton ($i = P$), *Trichodesmium* ($i = T$), detritus ($i = D$), DON ($i = \mathrm{DON}$) and other heterotrophs ($i = H$). The coefficient γ specifies the fraction of remineralization that goes directly to DIN. Note that all of the DON consumed by heterotrophs (presumably bacteria) not assimilated is remineralized directly to DIN. In (8):

$$U_P = \mu_P(1 - \mathrm{e}^{-I/I_P})(\mathrm{e}^{-I/I_{\beta P}})(\mathrm{DIN}/(\mathrm{DIN} + \mathrm{PKS})) \quad (9)$$

and

$$U_T = \mu_T(1 - \mathrm{e}^{-I/I_T})(\mathrm{e}^{-I/I_{\beta T}})(\mathrm{DIN}/(\mathrm{DIN} + \mathrm{TKS})), \quad (10)$$

which describe light- and DIN-dependent variations in phytoplankton and *Trichodesmium* DIN uptake. An exponential saturation function with photoinhibition is used to describe the light dependence (Platt et al., 1980), and a Michaelis–Menten hyperbolic saturation function is used to describe the N-dependence. In (9) and (10), μ_P and μ_T are the maximum growth rates, I_P and I_T are light saturation parameters, and $I_{\beta P}$ and $I_{\beta T}$ are photoinhibition parameters for phytoplankton and *Trichodesmium*, respectively. The variable I is the subsurface irradiance. In addition, in (9) and (10), PKS and TKS are half-saturation constants for DIN uptake for phytoplankton and *Trichodesmium*. Thus, as demonstrated by Carpenter and McCarthy (1975), *Trichodesmium* spp. take up DIN following Michaelis–Menten kinetics. Finally, although it has been shown that bacteria can utilize some forms of DIN directly (e.g., NH_4, Wheeler and Kirchman, 1986; Carlson and Ducklow, 1996), it is assumed here that direct heterotrophic utilization of DIN is negligible.

The growth equations for phytoplankton and *trichodesmium* are

$$\frac{\partial P}{\partial t} = \alpha U_P P - S_P P - h_P HC_\mathrm{m} P \quad (11)$$

and

$$\frac{\partial T}{\partial t} = \alpha G_T T - S_T T - h_T HC_\mathrm{m} T. \quad (12)$$

In (11) and (12), the first term represents growth, the second natural mortality and the third consumption by heterotrophs. The heterotrophic consumptive terms are defined above. Natural mortality is modeled using linear functions with mortality rates S_P and S_T for phytoplankton and *Trichodesmium*, respectively. These simple forms are used because there is very little known about the factors that control natural mortality of autotrophs in the ocean (there is, however, some evidence that autolysis may take place rather suddenly in *Trichodesmium* populations during summer (Devassy et al., 1978; Karl et al., 1992)). Light- and DIN-dependent phytoplankton growth in (11) is modeled using U_P as defined in (9), but *Trichodesmium* growth in (12) is modeled using

$$G_T = \mu_T(1 - e^{I/I_T})(e^{-I/I_{\beta T}}). \tag{13}$$

Thus, although *Trichodesmium* spp. take up DIN according to (10), their growth rate is not limited by DIN availability. Thus, when DIN concentrations are very low, *Trichodesmium* growth is supported almost entirely by N_2-fixation, and when DIN concentrations increase N_2-fixation is throttled back. Note also that there is no representation of phosphorus limitation in this model either; i.e., it is assumed that nitrogen fixation provides an infinite supply of nitrogen and that *Trichodesmium* is able to obtain or retain the phosphorus required to support growth that is controlled principally by the availability of light. The omission of P-limitation in the model is justified because the means by which *Trichodesmium* acquires the phosphorus needed for growth is currently unknown (Hood et al., 2000). It has been hypothesized that it may be obtained through vertical migration (Karl et al., 1992) or, alternatively, that it is derived from dissolved organic sources (A.F. Michaels, pers. comm.), but neither of these mechanisms has been proven.

An additional dimensionless coefficient α in (11) and (12) determines the fraction of photosynthesis that remains in particulate form with remainder $(1 - \alpha)$ partitioned to DON. This coefficient is included here because it has been shown that a significant fraction of the nitrogen (and carbon) fixed by phytoplankton and *Trichodesmium* is exuded as DON into the surrounding medium (e.g., Bronk et al., 1994; Glibert and Bronk, 1994; Capone et al., 1994; for DOC, Carlson et al., 1994).

Changes in DON concentration due to biological processes are modeled using an equation similar to (8):

$$\begin{aligned}\frac{\partial \mathrm{DON}}{\partial t} &= (1-\gamma)(\mathrm{ae}_P - \mathrm{ge}_P)h_P HC_\mathrm{m}P + (1-\gamma)(\mathrm{ae}_D - \mathrm{ge}_D)h_D HC_\mathrm{m}D \\ &\quad + (1-\gamma)(\mathrm{ae}_H - \mathrm{ge}_H)h_H HC_\mathrm{m}H + (1-\gamma)(\mathrm{ae}_T - \mathrm{ge}_T)h_T HC_\mathrm{m}T \\ &\quad + (1-\alpha)G_T T + (1-\alpha)U_P P + (1-\beta)S_P P + (1-\beta)S_T T \\ &\quad - Hh_{\mathrm{DON}}C_\mathrm{m}\,\mathrm{DON}.\end{aligned} \tag{14}$$

Here the positive terms with $1 - \gamma$ coefficients represent heterotrophic remineralization of particulate organic nitrogen to dissolved organic nitrogen, and the positive terms with $1 - \alpha$ coefficients represent direct contributions to the DON pool due to exudation by phytoplankton and *Trichodesmium*. There are also two additional DON source terms with $1 - \beta$ coefficients that represent contributions to the DON pool due to natural mortality of phytoplankton and *Trichodesmium*. The last term in (14) represents uptake of DON by heterotrophs such as bacteria and DON-consuming

protists. Thus, although it has been observed that some strictly autotrophic phytoplankton species are capable of utilizing DON (Cambella et al., 1984; Antia et al., 1991), it is assumed here that this process is negligible compared to heterotrophic uptake. It should be noted that DON in this model is consumed as readily as any other particulate organic constituent and should therefore be considered "labile".

Finally, changes in detritus concentration due to biological processes are modeled as follows:

$$\begin{aligned}\frac{\partial D}{\partial t} &= (1-\mathrm{ae}_P)h_P HC_\mathrm{m}P + (1-\mathrm{ae}_H)h_H HC_\mathrm{m}H \\ &\quad + (1-\mathrm{ae}_T)h_T HC_\mathrm{m}T + (1-\mathrm{ae}_D)h_D HC_\mathrm{m}D \\ &\quad + (1-\mathrm{ae}_{\mathrm{DON}})h_{\mathrm{DON}} HC_\mathrm{m}\,\mathrm{DON} + \beta S_P P + \beta S_T T \\ &\quad - h_D HC_\mathrm{m}D, \end{aligned} \tag{15}$$

where the terms with coefficients $(1-\mathrm{ae}_i)$ represent contributions to the detritus pool due to egestion by heterotrophs, and the terms with coefficients β represent contributions to the detritus pool due to natural mortality of phytoplankton and *Trichodesmium*. The only loss term in (15) represents consumption of detritus by heterotrophs. It should be noted that the egestion term in (15) due to DON consumption by heterotrophs is actually zero because the assimilation efficiency for DON is taken to be 1 (Table 1); i.e., it is assumed that there is no egestion associated with DON consumption.

The biological model is integrated numerically over time using a fourth-order Runge–Kutta scheme (Press et al., 1992).

2.2. Biological parameters

The parameters in the biological model used to generate the solutions discussed in Section 3 below are summarized in the top panel of Table 1. As stated above, the heterotrophic compartment in this model is considered to represent the sum of all heterotrophic processes in the pelagic environment in the upper 400 m of the water column in the Sargasso Sea. For the selection of parameters it is assumed that the heterotrophic consumption of organic matter is dominated by bacteria and microzooplankton, with mesozooplankton groups making a lesser contribution. Growth and assimilation efficiencies for consumption of phytoplankton, *Trichodesmium*, detritus and other heterotrophs were set at 0.20 and 0.70, respectively, to reflect the importance of microzooplankton in open-ocean ecosystems (Heinbokel, 1978; Verity, 1985). Similarly, for DON consumption a growth efficiency of 0.20 was used, which is within the range of accepted values for bacterial growth efficiencies (del Giorgio and Cole, 1998). Since there is no egestion associated with DON consumption by bacteria and protists, the assimilation efficiency for DON was set to 1. Size-dependent parameters for microzooplankton from Maloney and Field (1991) were used to set the maximum heterotrophic consumption rate and half-saturation constant at 6.4 d^{-1} and 0.80 mmol m^{-3}, respectively. For comparison, if a maximum bacterial growth rate of 2.0 d^{-1} is assumed (as in Fasham et al., 1990) then a growth efficiency of 0.20 gives a maximum bacterial DON consumption rate = 2.0/0.2 = 10, which is of the same order of magnitude as the C_m used

here. The heterotrophs are considered to consume phytoplankton, detritus, DON and other heterotrophs indiscriminantly ($\Phi_P = \Phi_D = \Phi_{DON} = \Phi_H = 1/4$), but it is assumed that *Trichodesmium* is not grazed to a significant extent by the bulk of the pelagic heterotrophs ($\Phi_T = 0$, O'Neil and Roman, 1994).

The phytoplankton light saturation parameter I_P ($= I_s$ in Platt et al., 1980) was set at 40 W m^{-2}, and the photoinhibition parameter $I_{\beta P}$($= I_b$ in Platt et al., 1980) was set at 400 W m^{-2} (cf., Table 2 in Platt et al., 1980). A value of 3.22 d^{-1} was used for the maximum phytoplankton growth rate, μ_P, which gives a maximum realized phytoplankton growth rate of 2.9 d^{-1} using the Platt et al. (1980) formulation (see their Eq. (4)). This maximum growth rate is in the mid-range of values predicted by the Eppley (1972) formula using mixed-layer temperatures observed at the BATS site. The half-saturation constant for phytoplankton DIN uptake, PKS, was set at 0.5 μmol m^{-3} following Fasham et al. (1990). The nitrogen-specific phytoplankton attenuation coefficient ($k_p = 0.0223$ m^2 $mmol^{-1}$ N) is equivalent to a chlorophyll-specific attenuation coefficient of 0.014 $m^2 mg^{-1}$ chlorophyll *a* (from Kirk, 1994) using a C:Chla (wt:wt) ratio of 50 (Parsons et al., 1984) and a C : N atomic ratio of 106:16 (Redfield et al., 1963).

For *Trichodesmium* the light saturation parameter I_T was set at 80 W m^{-2}, which is approximately equal to 400 μE m^{-2} s^{-1}, and it was assumed that photoinhibition is negligible under natural irradiance conditions, i.e., $I_{\beta T} = 0$ (Carpenter et al., 1993; D.G. Capone, unpublished data). The half-saturation constant for DIN uptake by *Trichodesmium*, TKS, was set equal to that of phytoplankton. Thus, it is assumed that *Trichodesmium* can take up some forms of DIN, such as NH_4^+, readily (Mulholland and Capone, 1999, but see also Carpenter and McCarthy, 1975). The maximum growth rate of *Trichodesmium* was set at 0.17 d^{-1}, which is the mid-range of the observed rates (measured doubling times range from 3 to 5 d, Capone et al., 1997). For simplicity it is assumed that the nitrogen-specific *Trichodesmium* attenuation coefficient is the same as that of phytoplankton.

Following Fasham et al. (1990), 75% of the excretion by heterotrophs is released in the form of DIN ($\gamma = 0.75$), e.g., NH_4, with the remaining 25% released as DON ($1 - \gamma = 0.25$), such as urea. In addition, it is assumed that 25% of the nitrogen released due to natural mortality of phytoplankton and *Trichodesmium* contributes directly to the detritus pool ($\beta = 0.25$), with the remaining 75% contributing directly to the DON pool ($1 - \beta = 0.75$). As discussed above, recent work has shown that direct exudation of DON by phytoplankton generally constitutes a significant fraction (25–41%) of the DIN taken up by phytoplankton (Bronk et al., 1994), and similarly high-release fractions have been observed for *Trichodesmium* (Glibert and Bronk, 1994; Capone et al., 1994). The coefficient α, which partitions phytoplankton and *Trichodesmium* production between particulate and dissolved forms, was therefore set at 0.70, i.e., 30% of the DIN uptake is released as DON.

The three remaining biological parameters, the sinking rate of detritus, *w*, and the natural mortality coefficients for phytoplankton, S_P, and *Trichodesmium*, S_T, are not well constrained by observations. We therefore set $S_P = 0.01$ and used different combinations of *w* and S_T to tune the model to generate the high N_2-fixation and low N_2-fixation solutions described in Section 3.2.

2.3. CO_2 chemistry and air–sea exchange

The carbon system is modeled by incorporating one additional model compartment for DIC (Fig. 1). The effects of biological processes on DIC are accounted for by assuming that the

autotrophic uptake and heterotrophic release of aqueous CO_2 are proportional to the uptake and release of DIN. Thus, the cycling of carbon through the pelagic ecosystem is not explicitly modeled. Rather, it is assumed to cycle in parallel with nitrogen. CO_2 is taken up by phytoplankton and *Trichodesmium* and released through heterotrophic metabolism. A C : N ratio of 10 was used for the main-run solutions presented in this paper because the C : N ratio of sinking particulate material approaches this value in particulate material caught in sediment traps below the euphotic zone at BATS (A.F. Michaels, pers. comm.). This is justified because the primary goal of this paper is to estimate rates of N_2-fixation that are critically dependent upon the C : N ratio of the exported material. If carbon export is calculated using a C : N ratio of 6.625 (Redfield et al., 1963), the model will tend to overestimate the amount of nitrogen export that is required to lower the DIC concentrations in the upper ocean to the observed levels. This, in turn, will result in a higher estimate of the input of atmospheric nitrogen that is required from N_2-fixation to balance the nitrogen export at depth.

In this model, the C : N ratio has to be the same for all components of the ecosystem and at all depths. Thus, running the model with a C : N ratio of 10 may result in overestimation of DIC uptake in the surface waters by *Trichodesmium* and phytoplankton in general. It is well known that the average C : N ratio of living organic matter is about 6.625 (Redfield et al., 1963) and it has been shown that the C : N ratio of *Trichodesmium* may be somewhat lower (C : N $\approx$ 5–6.5, Carpenter et al., 1993; Letelier and Karl, 1996). However, Sambrotto et al. (1993) have shown that the ratio of consumption of inorganic carbon and nitrogen in surface waters of the North Atlantic ocean tends to be significantly higher than Redfield, with uptake C : N varying from about 8 to 15. These observations are consistent with the C : N ratio of remineralization in the upper thermocline at BATS, which may be as high as 16 (A.F. Michaels, pers. comm.). Thus, running the model with a C : N ratio of 10 appears to be an appropriate and relatively conservative choice. The effect of using different C : N ratios on the model-estimated rates of N_2-fixation is discussed in Section 3.3.

Mixed-layer DIC is also affected by the CO_2 flux across the air–sea interface. This flux is modeled as a function of wind speed and ΔpCO_2, using the relation proposed by Tans et al. (1990). This formulation, which gives exchange rates similar to those calculated using Wanninkhof's (1992) equation, was chosen for its simplicity. Moisture-corrected atmospheric pCO_2 is prescribed using measured dry air concentrations from Bermuda that were collected as part of the NOAA/CMDL global cooperative air sampling network. Exchange of DIC with the deep ocean occurs in parallel with DIN, i.e., through turbulent diffusive exchange and the sinking export of detritus. The effect of all of the above processes on the chemistry of CO_2 system and pCO_2 in seawater is determined using the chemical model recommended by UNESCO (1987) which uses the carbonic acid dissociation constants of Dickson and Millero (1987) fit to the pooled data of Mehrbach et al. (1973) and Hansson (1973). The expression used for the solubility of CO_2 in seawater is from Weiss (1974) and the dissociations of boric acid and water are modeled following Millero (1979).

The carbon system model calculates the new equilibrium pCO_2 given a change in DIC concentration when aqueous CO_2 is taken up or given off by biological processes or exchanged either at the sea surface or the deep-ocean boundary. It also accounts for the effects of temperature and pressure on the CO_2 system. Although biological processes in the ocean can modify the total alkalinity (TALK) of seawater and pCO_2 through the formation and dissolution of calcium carbonate and the uptake and release of NO_3 and NH_4 (Brewer and Goldman, 1976), these effects are not explicitly considered in this model. The latter is justified because the proton budget is not

important in the Sargasso Sea where the seasonal changes in nitrogen concentrations in the surface waters are small (i.e., less than 1 mmol m^{-3}). Although calcite formation can have a significant effect upon TALK at BATS (e.g., Bates et al., 1996, their Fig. 8), it is not explicitly modeled here because, at present, it is not possible to model dynamically or predict calcite formation in the ocean (this is a major unresolved problem, widely recognized by the biogeochemical modeling community; Sarmiento and Armstrong, 1997). Fortunately, calcification events are rare in the Sargasso Sea; only two have been observed over the last 10 yrs (Bates et al., 1996; N.R. Bates, unpublished observations). Analysis of salinity-normalized TALK suggests that there is interannual variability of few μmol kg^{-1}, which represents a change in TALK of less than 0.2% (Bates, 2001). It is therefore assumed that TALK is a conservative tracer of salinity and it is estimated using an empirically derived relationship from Bates et al. (1996):

$$\mathrm{TALK} = -47.155 + 66.576\mathrm{Salinity}, \quad r^2 = 0.91, \tag{16}$$

which describes the relationship between TALK and salinity in the mixed layer at BATS.

2.4. *Mixing, diffusion, sinking and light*

All of the compartments in the biological model are subjected to physical mixing processes simulated using a modified version of the Price et al. (1986) mixed-layer model. Briefly, in this model vertical mixing is carried out in order to satisfy three different stability criteria. Mixing occurs when heat and/or freshwater exchange at the sea surface results in gravitational instability (i.e., when the density, ρ, is distributed such that $\partial\rho/\partial z < 0$), and when shear at the base of the mixed layer and/or in the upper thermocline is sufficient to cause turbulent entrainment (i.e., when the bulk and/or gradient Richardson numbers exceed critical values).

The mixed-layer model also allows the application of a background diffusion. This option is an important aspect of this implementation of the Price et al. model because diffusion is the only mechanism that brings DIN and DIC up through the thermocline from the deep ocean. In the simulations described below diffusion was applied uniformly below the mixed layer to parameterize turbulent transport in the upper thermocline using $K_w = 0.0001$ m^2 s^{-1} (Table 1). This value is about an order of magnitude higher than values derived from die release experiments in the eastern North Atlantic ($K_w = 0.000012$–0.000017 m^2 s^{-1}, Ledwell et al., 1998). The higher value is used here because it gives DIN and DIC concentrations that compare much more favorably with the BATS observations. In particular, when the model is run with the Ledwell et al. K_w values, it substantially underestimates the near-surface DIC concentrations in late winter/early spring. It is critical to reproduce these initial pools as accurately as possible because the model-estimated annual N_2-fixation rate and phytoplankton production rate are strongly influenced by the DIC and DIN concentrations (respectively) in the euphotic zone at the beginning of the season. The high K_w used here is roughly consistent with values inferred from excess ^{3}He in the upper ocean near Bermuda (Jenkins, 1988) and, as Jenkins points out, likely reflects the influence of isopycnal and mesoscale processes. The importance of the latter has been recently confirmed by modeling studies that suggest that eddy-induced fluctuations in the depth of the nitracline can drive a significant net vertical nitrate (and presumably also DIC) flux (McGillicuddy and Robinson, 1997; McGillicuddy et al., 1998). Thus, setting $K_w = 0.0001$ m^2 s^{-1} should be considered as a crude parameterization

of these processes. The effect of using the Ledwell et al. K_w values on the model-estimated N_2-fixation rate is discussed in Section 3.3.

Diffusive flux is calculated in the model using a Crank–Nicholson numerical scheme (Press et al., 1992). The Price et al. (1986) model has also been modified to allow sinking of detritus. This is done using a vertical advection equation which is solved numerically using a positive-definite scheme (Smolarkiewicz, 1983).

The bottom boundary of the model is open for all biological and chemical constituents except phytoplankton, *Trichodesmium* and heterotrophs, the biomasses of which are assumed to be confined within the 400 m model domain. The sinking flux of detritus out of the bottom boundary is controlled by the sinking rate of detritus, w, and the detritus concentration calculated by the model immediately above the bottom. The diffusive fluxes of salinity, temperature, DIN and DIC are controlled independently by the thermocline diffusivity and the gradients across the bottom boundary, which are set using model-predicted concentrations immediately above the bottom and the observed BATS salinity, temperature, DIN and DIC concentrations interpolated to the 400 m boundary. DON is treated similarly except that the labile DON concentration below 400 m is taken to be zero. CO_2 is exchanged at the sea surface using the air–sea flux formulations and boundary conditions described above.

Absorption of solar radiation in the Price et al. (1986) model is simulated using a double exponential decay equation:

$$I_Z = I_0[R\mathrm{e}^{-k_1 Z} + (1 - R)\mathrm{e}^{-k_2 Z}], \tag{17}$$

where I_Z and I_0 are instantaneous surface and subsurface solar insolations, R and $(1 - R)$ are the long- and shortwave components of the insolation, and k_1 and k_2 are the long- and shortwave diffuse attenuation coefficients, respectively. To incorporate the effects of light absorption by phytoplankton, the model has been modified so that

$$k_2 = k_x + k_\mathrm{p}(P + T). \tag{18}$$

Here k_x is the diffuse attenuation coefficient for water and substances other than phytoplankton and *Trichodesmium*, and k_p is the biomass-specific attenuation coefficient defined above. Thus, phytoplankton and *Trichodesmium* attenuate the shortwave radiation, but attenuation of longwave radiation is considered to be negligible compared to water. In addition, it is assumed that 90% of the light which is absorbed by phytoplankton is re-radiated back into the water as heat (Kirk, 1994). Thus, the primary effect of the phytoplankton is to change the vertical distribution of heating of the water by shortwave radiation.

2.5. Forcing, restoration and initialization

The model is forced at the sea surface using synoptic data from the Bermuda airport collected between January 1, 1989 and December 31, 1997. This meteorological station is located about 70 km NW of the BATS site. These data are used for this application because large-scale forcing sets, such as ECMWF and COADS, tend to represent poorly the upper and lower extremes of

distributions found in the direct observations (Doney, 1996), which are required to calculate air–sea exchange of CO_2 correctly (Bates et al., 1998). Net shortwave radiation, Q_{sw}^{net}, is calculated using Dobson and Smith's (1988) "Okta" model as recommended by Bishop and Rossow (1991). This is an hourly model, which determines net shortwave radiation at the sea surface using the solar constant and solar elevation calculated using standard astronomical formulae. Thus, it includes both seasonal and diel variability. In Dobson and Smith's model, atmospheric transmission is calculated using an empirical relationship between transmission and observed cloud cover. The Q_{sw}^{net} also forces the ecosystem model directly through (9), (10), (13) and (17). Following Doney (1996), the net longwave radiation, Q_{lw}^{net}, is calculated using the conventional bulk blackbody radiation formula of Berliand and Berliand (Fung et al., 1984). However, for this application atmospheric transmission for the Berliand and Berliand formula is calculated using Dobson and Smith's (1988) empirical relationship. The turbulent heat fluxes, Q_{sen} and Q_{lat}, are computed from standard air–sea transfer equations (Large and Pond, 1982) using air and dewpoint temperatures measured at the Bermuda airport and sea-surface temperatures measured at BATS. The x- and y-directed wind stresses are computed using the airport-measured wind speed and direction and a traditional bulk turbulent formula (Large and Pond, 1982). Finally, the net air–sea freshwater flux was calculated using 6-hourly cumulative precipitation measurements from the Bermuda airport and evaporation from Q_{lat}.

The annual surface heat and freshwater fluxes are, on average, not balanced at the BATS site (Doney, 1996); i.e., there are significant net surface heat and freshwater losses that must be compensated for by horizontal advection. In order to balance these surface losses in the model, temperature and salinity are restored to the observed values using a simple "nudging" technique. The presence of a net horizontal flux of heat into the region also implies a net flux of DIN and DIC. However, it is not possible to account for this advective flux by similarly restoring DIN and DIC concentrations to the observed values because there is no way to determine if differences between the model-generated and observed DIN and DIC are the result of horizontal fluxes or incorrect model dynamics; i.e., if the biological and chemical model results are significantly in error the restoration scheme will generate fluxes to compensate which have nothing to do with reality. Therefore, DIN and DIC are not restored in this application.

The model is initialized on January 1, 1989 using BATS temperature, salinity, DIN ($NO_3 + NO_2$) and DIC data that were interpolated to the first of the year. For both solutions described in Section 3, the biological state variables P, T, H,DON and D are initialized at low and vertically uniform concentrations (0.03 mmol m^{-3} for P, H, DON and D, and 0.005 mmol m^{-3} for T). The model is then spun up for three years before proceeding forward in time from January 1, 1989.

2.6. Physical parameters

With a few exceptions the mixed-layer model parameters are set as in Price et al. (1986, see their Section 4.0). All of the parameters that have been altered from those in Price et al. (1986) and the additional parameters associated with modifications to the mixed-layer model described above are listed in the bottom panel of Table 1.

For the runs in this paper the time step is 3600 s. In Eq. (12), k_x is set at 0.03 m^{-1} assuming that the attenuation of shortwave radiation by water and substances other than phytoplankton

approaches that of the clearest open-ocean waters (Kirk, 1994; his Table 6.1). The restoration time scales for temperature and salinity, T_T and T_S, are both set at 41.66 d to maximize agreement between the observations and the modeled mixed-layer cycles, surface temperature and surface salinity.

2.7. Data sets

Data sets collected as part of the US JGOFS BATS sampling program are used extensively in the analysis described below. These measurements include CTD temperature and salinity, which were used to restore the model-generated temperature and salinity fields and calculate σ_t for estimating mixed-layer depths (the latter was taken to be the depth at which the change in σ_t over 1 m depth exceeds 0.001). In addition, the BATS DIC, DIN ($NO_3 + NO_2$), particulate ^{14}C primary production and export flux of particulate nitrogen at 300 m (as measured by sediment traps) are used for comparison with the model results. The methods used to make these measurements are described in Knap et al. (1993). All of the data used here were downloaded directly from BATS web site (http://www.bbsr.edu/bats/batsdata.html). A series of data reports describing the data sets is also available (see reports by Knap et al. at http://www.bbsr.edu/bats/batsdata.html).

The atmospheric forcing data from the Bermuda Airport were obtained from the National Climatic Data Center.

3. Results and discussion

3.1. Forcing and mixed-layer response

The 24-h averaged surface heat fluxes, wind stress, evaporation and precipitation derived from the Bermuda Airport meteorological observations are shown in Fig. 2. Perhaps the most striking feature of this forcing set is the amount of high-frequency variability observed in the surface heat losses, wind stress and precipitation. Much of the variability in the total surface heat loss derives from the wind because the sensible and latent fluxes are multiplied by wind speed in the bulk formulae (Large and Pond, 1982, their Eq. (8)). Note, in particular, the strong wind stress and precipitation events in the summer and fall of 1995, which was, by far, the most active hurricane year in the record. Significant wind and/or precipitation anomalies were recorded in association with hurricanes Felix (August 14 and 15), Luis (September 9 and 10) and Marilyn (September 18 and 19).

Panels A and B of Fig. 3 show that the observed variations in sea-surface temperature (SST) and mixed-layer depth (MLD) are estimated quite well by the mixed-layer model. In general, SST is within 1°C of the observations except in some specific cases, e.g., during the summers of 1991, 1994 and 1995, and during the winter of 1989–1990 when the model-predicted surface temperatures were lower than observed. In the summer of 1995 the discrepancy appears to be the result of slow restratification following storm events, i.e., Hurricane Felix. Because the absolute mixed-layer depths from the BATS observations are a function of the criterion used to calculate them, it is most appropriate to compare interannual variations. In general, the year-to-year variations in the depth of winter mixing predicted by the model coincide with the observations. However, it appears that in

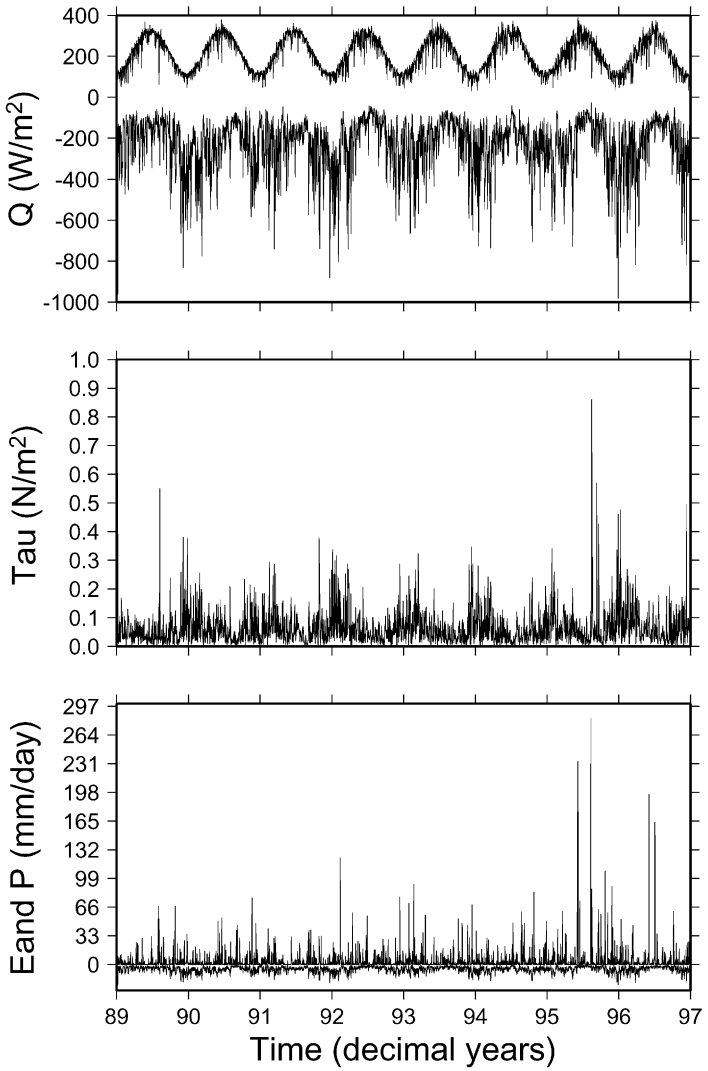

Fig. 2. Daily averaged surface forcing functions derived from the Bermuda Airport synoptic meteorological observations. Freshwater fluxes are plotted in the bottom panel with positive values representing precipitation and negative values evaporation. The surface wind stress is plotted in the middle panel. In the top panel the positive values are the net shortwave radiation, Q_{sw}^{net}, and the negative values are the sum of the net longwave radiation, Q_{lw}^{net}, and the sensible, Q_{sen}, and latent, Q_{lat}, heat fluxes.

1990, 1991 and, perhaps, in 1992 the model penetrates too deeply in late winter and the model has a general tendency to shoal somewhat late, e.g. in 1990, 1991 and 1994–1996. The latter may be due to the fact that there is an inherent time lag in the restoration scheme used here, which replaces heat and freshwater lost to the atmosphere over a period of about 1.5 months. This lag, which is also apparent when the mixed layer is deepening, is reflected in SST to some extent as well, e.g., in 1990 and 1991.

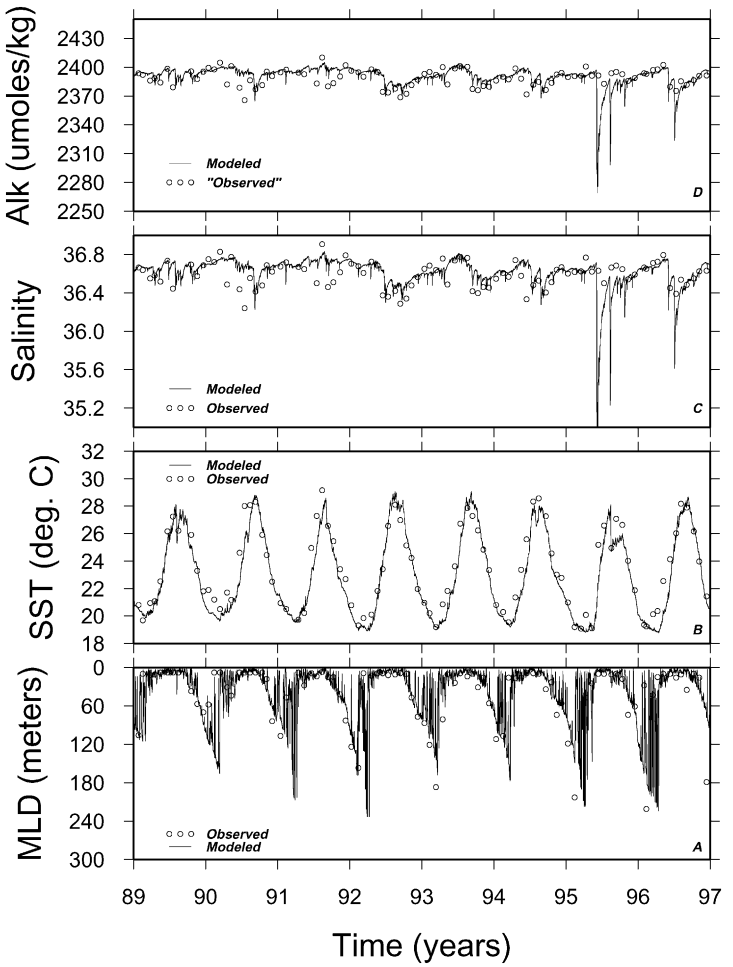

Fig. 3. Comparison of BATS observations with model-estimated (A) noon-time mixed-layer depth (MLD), (B) sea-surface temperature (SST), (C) sea-surface salinity and (D) TALK estimated from model-predicted and BATS observed CTD salinities using the Bates et al. (1996) empirical salinity vs. TALK relationship (see Section 3.1 in the text for details).

Panel C of Fig. 3 shows that salinity is generally predicted to within 0.4 salinity units except in a few extreme cases. In particular, the model consistently predicts lower salinities during hurricane- and storm-related precipitation events in 1995 and 1996. For example, in the summer of 1995 the model salinity drops below 35.4 twice in response to two major precipitation events (see Fig. 2), whereas the observed salinity never drops below 36.4. This apparent discrepancy may be largely because post-storm sampling was usually at least several days after each event. In all cases the model salinity returns to near pre-storm levels by the time of the direct measurement. Thus, the model may be estimating the surface salinity during the storm events reasonably well. Because TALK is calculated using an empirical relationship with salinity, differences in the predicted and observed salinities translate directly to differences in TALK. Panel D in Fig. 3, which compares

Table 2
Errors associated with model-predicted physical and chemical parameters involved in calculating pCO_2 and resulting pCO_2 precision

Parameter	Approx. model error	Calculated pCO_2 precision[a] (μatm)
Temperature	$\pm 1^{\circ}C$	± 15
Salinity	± 0.4	± 3
Alkalinity	± 20 μmol kg^{-1}	± 25
DIC	± 20 μmol kg^{-1}	± 30

[a]Calculated at 1 m depth, 24°C, 36.6 salinity, 2387 μmol kg^{-1} alkalinity, and 2040 μmol kg^{-1} DIC.

TALK calculated from the model-predicted salinity to TALK calculated from the BATS salinity observations, reveals that differences in the predicted and the "observed" values are usually less than 20 μmol kg^{-1} except during the precipitation events in 1995 and 1996. Errors in the TALK prediction associated with uncertainties in the Bates et al. (1996) salinity vs. TALK relationship should generally be within 3 μmol kg^{-1} except during major calcification events (see Bates et al., 1996, their Fig. 8a).

Since temperature, salinity, TALK and DIC concentrations are all utilized in the calculation of the surface pCO_2, any errors in the model-predicted values will directly impact the calculated air–sea CO_2 exchange. Table 2, which shows the magnitude of the pCO_2 changes that result from the errors discussed above and assuming a precision of ± 20 μmol kg^{-1} for DIC (see below), suggests that errors in TALK and DIC have the largest impact on the calculated pCO_2 values (± 25–30 μatm). However, many of the differences between the modeled and observed values can arise as a result of differences in the timing of sampling and manipulation of the data sets, e.g., as discussed above with salinity. The BATS data sets are not error-free, and the model-generated and observed data sets are not entirely comparable. Thus, the "model errors" in Table 2 should be considered conservative estimates. Nonetheless, Table 2 suggests that efforts to improve the model's salinity/TALK prediction would be well placed and that care should also be taken to predict surface DIC concentrations as accurately as possible (see below).

3.2. N_2-fixation variability and effect on C and N concentrations and fluxes

In this section two model solutions are presented and contrasted. In solution 1 the nitrogen fixation rate of *Trichodesmium* was adjusted to give the best possible simulation of the subsurface DIC concentrations and primary productivity. In contrast, in solution 2 the nitrogen fixation rate was adjusted to give the best possible simulation of the nitrogen export flux at 300-m and primary productivity. Thus, in solution 1 the model was constrained to fit the observed DIC concentrations and the 300-m N flux was unconstrained, whereas in solution 2 the model was constrained to fit the observed 300-m flux and DIC was unconstrained.

This tuning was done by adjusting two model parameters: the *Trichodesmium* mortality rate, S_T, and the sinking rate of detritus, w. These two parameters are changed simultaneously because they have compensatory effects in the model. In order to simulate the summertime DIC concentrations

at BATS, it is necessary to decrease S_T to 0.021 d^{-1} to give summertime N_2-fixation rates high enough to lower DIC to the observed values. However, with these high rates of N_2-fixation it is also necessary to increase w to 12 m d^{-1}, which increases the nitrogen export flux and maintains production rates at the observed levels. If w is not increased, production rates increase dramatically and nitrogen accumulates in the model domain because combined nitrogen influx from the atmosphere due to N_2-fixation exceeds export at depth. In contrast, to simulate the observed 300-m nitrogen export fluxes it is necessary to lower w to 4 m d^{-1}. But with this lower export, it is also necessary to increase S_T to 0.0235 to lower the N_2-fixation rates to maintain the observed production rates. If S_T is not increased, production rates tend to increase to unrealistically high levels, and, again, nitrogen accumulates in the model domain because N_2 influx from the atmosphere exceeds export at depth.

It is shown below that solutions 1 and 2 are similar in many respects and quite different in others. In particular, solutions 1 and 2 give radically different estimates of what the nitrogen fixation rates should be at BATS.

3.2.1. Trichodesmium biomass and nitrogen fixation

(In the remaining sections solution 1 is also referred to as S1 and/or the high N_2-fixation solution and solution 2 is referred to as S2 and/or the low N_2-fixation solution.)

Fig. 4 shows the interannual variability in *Trichodesmium* biomass and the vertically integrated nitrogen fixation rates for solutions 1 and 2, respectively. In both plots it can be seen that the model predicts strong seasonal variations in N_2-fixation and biomass, with maximum rates developing in late summer/early fall and maximum biomass developing slightly later. Note also that most of the *Trichodesmium* biomass is confined to the upper 50 m of the water column and extends deeper only during periods of deep mixing/entrainment. Thus, the patterns predicted by this simple *Trichodesmium* model are basically similar to the patterns that are observed in situ; *Trichodesmium* biomass and N_2-fixation are generally confined to the upper 50 m of the water column (Mague et al., 1977; Carpenter, 1983; Letelier and Karl, 1996; Capone et al., 1997), and at BATS peak rates and biomasses develop in late summer/early fall when the water column is stratified and are lowest during late winter and early spring when deep mixing occurs (Orcutt et al., 2001). Although it is generally believed that the natural bouyancy of *Trichodesmium* contributes to their localization in near-surface waters (Walsby, 1992; Villareal and Carpenter, 1990; Romans and Carpenter, 1994), the model suggests that the depth distribution of *Trichodesmium* is restricted to the upper water column primarily because they grow near the surface; i.e., unlike phytoplankton, their growth is not constrained by the upward diffusion of DIN and they are less photoinhibited at high irradiances.

The seasonal patterns appear to be driven by a combination of light availability, which is modified by competition with phytoplankton, and growth-restricted biomass accumulation; i.e., N_2-fixation rates and *Trichodesmium* biomass drop to the lowest levels in late winter/early spring is when the surface irradiance is low, the water column is mixed and the mean light levels are lowest. During this period *Trichodesmium's* natural mortality rate, S_T, exceeds its light-limited growth rate. When the mixed layer shoals in spring, the *Trichodesmium* population does not immediately increase because it grows slowly and is outcompeted by phytoplankton for light. The *Trichodesmium* biomass begins to accumulate only after the spring phytoplankton bloom crashes (compare Fig. 4 with 7). *Trichodesmium* increases during summer when phytoplankton growth at the surface is strongly nutrient-limited. This is also the time period when the surface irradiance is high and the

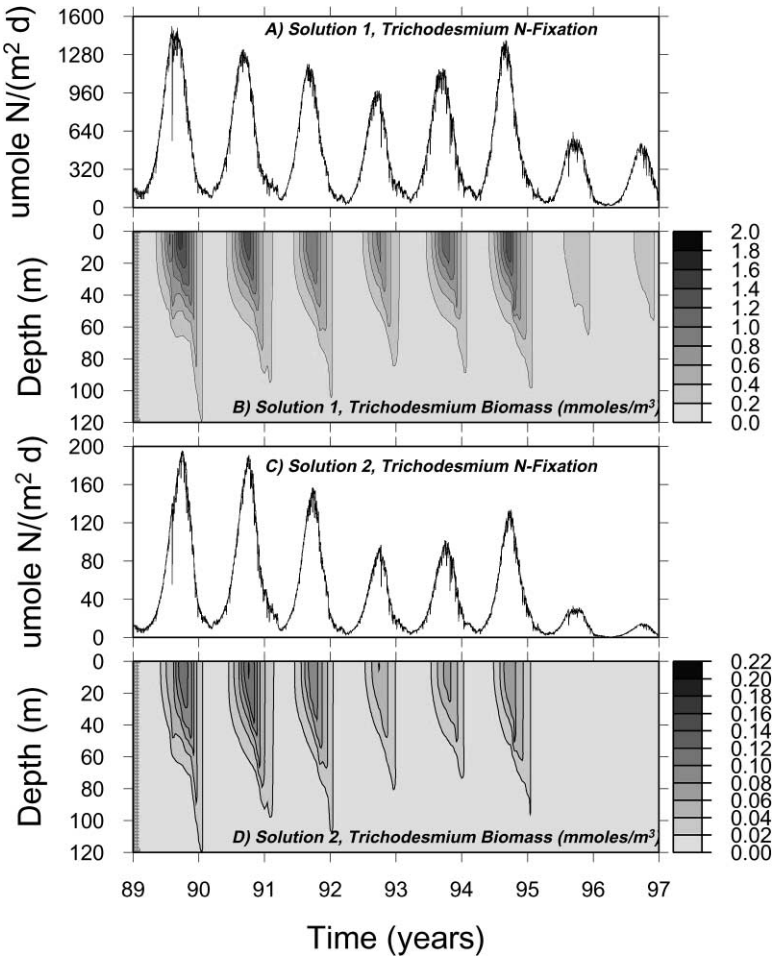

Fig. 4. Model-estimated subsurface *Trichodesmium* concentration and vertically integrated N_2-fixation rate for the solution tuned to reproduce the observed DIC concentrations and primary production (S1, panels A and B), and the solution tuned to reproduce the 300-m sediment trap fluxes and primary production (S2, panels C and D).

mixed layer is thin, resulting in the highest mean light availability in the upper water column. This maximizes *Trichodesmium*'*s* growth rate. The population reaches its peak in late summer/early fall after the biomass has had time to accumulate. Then in late fall the population is dispersed vertically by winter mixing, which lowers the light levels once again.

Fig. 4 also shows that the model generates strong interannual variations in *Trichodesmium* biomass and N_2-fixation: The highest rates and biomasses are generated in 1989, decrease through 1992, increase again in 1993 and 1994, then drop precipitously in 1995 and 1996. These interannual variations are roughly inversely related to interannual variations in the depth and duration of winter mixing (compare Fig. 3A with 4) and the strength of the spring phytoplankton bloom (compare Fig. 4 with 7), i.e., in years when there is deeper and/or more prolonged mixing and

a stronger phytoplankton bloom *Trichodesmium* biomass and N_2-fixation rates tend to be lower during the following late summer/early fall. Increased winter mixing strengthens the phytoplankton bloom because it increases the nutrient supply that supports the bloom. In contrast, deep mixing in winter and a strong phytoplankton bloom in spring result in lower light levels, which reduces *Trichodesmium* biomass at the beginning of the *Trichodesmium* growing season. Because *Trichodesmium* grows very slowly, small changes in the initial biomass translate into large differences during late summer/early fall. This dynamic can be thought of as a simple competative interaction: When phytoplankton do well, *Trichodesmium* does not and vice versa, and the commodity for which they are competing is light.

However, the sharply lower N_2-fixation rates and *Trichodesmium* biomasses in 1995 and 1996 are due, at least in part, to the exceptionally stormy summer of 1995 (see Fig. 2); i.e., it appears that unusually strong wind events and associated mixing during the summer of 1995 prevent the full development of the *Trichodesmium* population that year. As a result the initial biomass in 1996 is unusually low. This, in combination with stormier than average conditions in the summer of 1996, results in reduced *Trichodesmium* population in 1996 as well. Note also that winter mixing was relatively deep and prolonged (Fig. 3A) and the spring phytoplankton bloom was strong (Fig. 7) in both 1995 and 1996, which likely also contributed to the lower N_2-fixation rates and *Trichodesmium* biomasses in these two years.

Trichodesmium populations have not been routinely monitored at BATS. However, in the time period 1995–1997 Orcutt et al. (2001) observed lower rates and colony abundances in 1995 and 1997, and substantially higher rates in 1996. Thus, unlike the model results, it appears that *Trichodesmium* population was much reduced in 1995 and recovered substantially in 1996. This discrepancy between the model and the observations could be due to the fact that the model does not allow for horizontal advection of *Trichodesmium* from adjacent regions, which may help the population at BATS recover following low-abundance years. Although there are not sufficient data available to determine whether or not 1995 and 1996 were actually low *Trichodesmium* years compared to previous years, it is interesting to note that the highest biomass measurements made by Orcutt et al. (2001) in 1996 ($\approx$ 200 colonies m^{-3}) are about 5 times lower than measurements made in the same region in 1990 by Carpenter and Romans (1991) ($\approx$ 1000 colonies m^{-3}, see their Fig. 2). This is roughly the same biomass difference generated by the model in solutions 1 and 2 between 1990 and 1996.

Although qualitatively the seasonal, interannual and depth distribution patterns are very similar in S1 and S2 (Fig. 4), the absolute rates and biomasses are dramatically different (note the differences in the scales). In S1, where the N_2-fixation rate was adjusted to levels that give approximately the correct summertime DIC concentrations, the maximum summertime rates vary between 500 and 1500 μmol N m^{-2} d^{-1}, with maximum biomasses between 0.2 and 2 mmol m^{-3}, with the lower values corresponding to 1995 and 1996. In contrast in S2, where the N_2-fixation rates were adjusted to give the correct export flux at 300 m, the summertime rates vary between about 20 and 200 μmol N m^{-2} d^{-1}, with the biomasses between 0.02 and 0.2 mmol N m^{-3}, again with the lower values corresponding to 1995 and 1996. Thus, the two solutions predict N_2-fixation rates and *Trichodesmium* biomasses that differ by approximately an order of magnitude.

For comparison, Orcutt et al. (2001) measurements suggest maximum total summertime N_2-fixation rates of about 20–200 μmol N m^{-2} d^{-1} and maximum *Trichodesmium* biomass of about

0.03–0.3 mmol N m^{-3}, depending upon the assumed percentage of the population that occurs as free trichomes (the lower end of the ranges assume 0% free, whereas the higher end represents 90% free). Observations from 1990 in the Sargasso Sea reported by Carpenter and Romans (1991) suggest summertime N_2-fixation rates of $\approx$ 700–1400 μmol N m^{-2} d^{-1} and biomass of $\approx$ 0.14–0.28 mmol N m^{-3} for colonies alone (see also Lipschultz and Owens, 1996). In contrast, average rate estimates from two studies carried out in the 1970s in subtropical Atlantic waters gave means of 1.4 ± 0.47 μmol N m^{-2} d^{-1} (s.e., for 9 stations, Carpenter and McCarthy, 1975) and 6.2 ± 4.0 μmol N m^{-2} d^{-1} (s.e., for 7 stations, Carpenter and Price, 1977). Thus, the Orcutt et al. biomass observations from 1996 are in agreement with the S2 values for 1995–1996 if it is assumed that the contribution from free trichomes is negligible, whereas they are in agreement with the S1 values if it is assumed, as Orcutt et al. (2001) argue, that a large fraction of the population is free. The Carpenter and Romans (1991) rate estimates are approximately in agreement with the S1 values for 1990, and they imply even higher rates if a significant proportion of the population exists as free trichomes. However, their biomass estimates are more in line with the S2 values. In contrast, the rate estimates from the 1970s (from Carpenter and McCarthy, 1975; Carpenter and Price, 1977) are at least an order of magnitude lower than any of the above values.

(Note: The averages from the 1970s may be somewhat misleading as the actual range of rates observed by Carpenter and McCarthy (1975) spanned two orders of magnitude due to the spatial heterogeneity and variable N_2-fixing activity of *Trichodesmium*. These older estimates also used an empirically derived ratio to derive N_2-fixation rates from acetylene reduction that was probably low by a factor of 2. Nonetheless, these rate estimates would have to be low by at least a factor of 10 to bring them into agreement with S2, and they would have to be low by at least a factor of 100 to bring them into agreement with S1.)

Table 3 reveals the same patterns that are apparent in Fig. 4: generally higher rates from 1989 to 1994 and a difference of about a factor of 10 between S1 and S2. In addition, Table 3 shows that the annual rates from S1 for 1989–1994 (136–242 mmol N m^{-3} yr^{-1}) agree quite well with the geochemical rate estimates from Michaels et al. (1996). The rate estimates from Carpenter and Romans (1991) are also in agreement with S1 if it is assumed that the summertime N_2-fixation rates are maintained over 6 months of the year. The annual N_2-fixation rate estimate of Gruber and Sarmiento (1997) is closest to the S1 values predicted by the model for 1995–1996, and the Orcutt et al. average annual N_2-fixation rate estimate for 1995–1997 is lower still, lying in between the S1 and S2 estimates for 1995–1996. If it is assumed that there are no seasonal variations in N_2-fixation, then the direct measurements from the 1970s agree most closely with the rates from S2 for 1995–1996.

Thus, the model solution with N_2-fixation adjusted to give the correct summertime DIC concentrations (S1) gives rates that are generally consistent with the geochemical estimates whereas the solution adjusted to agree with the 300-m sediment trap fluxes (S2) gives rates that are lower than the geochemical estimates by at least a factor of 3. It is difficult to determine which of the model solutions agrees best with the direct rate and biomass estimates for the North Atlantic because the direct rate and biomass estimates are extremely variable; i.e., they range from 0.5 to 256 mmol N m^{-2} yr^{-1} (Table 3). This comparison is further confounded by interannual variability in the model-predicted rates. However, the difference between the colony concentrations reported by Orcutt et al. (2001) and Carpenter and Romans (1991) is consistent with both S1 and S2 and suggests that N_2-fixation rates at BATS were, indeed, much higher in 1990 than they were in

Table 3
Integrated annual N_2-fixation rates for the BATS site computed from model solutions 1 and 2 for each year and compared to direct and indirect rate estimates from various sources

Year	Solution 1	Solution 2
	(mmol N m^{-2} yr^{-1})	
1989	242	27
1990	204	26
1991	176	22
1992	136	12
1993	177	14
1994	201	18
1995	91	5.4
1996	71	1.9
Model 1989–1994 mean	189	20
Model 1995–1996 mean	81	3.6
Michaels et al. (1996)[a]	133–230	
Gruber and Sarmiento (1997)[b]	72	
Derived from Carpenter and Romans (1991)[c]	128–256	
Orcutt et al. (2001)[d]	25	
Derived from Carpenter and McCarthy (1975)[e]	0.5	
Derived from Carpenter and Romans (1977)[e]	2.26	

[a]Based on vertical N* distribution at BATS.
[b]Based on vertical N* distribution from 10° to 50°N and 90° to 10°W.
[c]Based upon concentrations of 1000–2000 colonies m^{-3} measured in the western Atlantic in 1990 between 29° and 32°N and assuming a uniform 50 m vertical distribution and a 6 month growing season.
[d]Based upon colony concentrations and direct rate measurements at BATS from 1995 to 1997 and including contributions from free trichomes.
[e]Based on a range of estimated rates from the 1970s for a suite of stations from 23° to 36°N in the Sargasso Sea and assuming no seasonal variations.

1995–1997. According to the model, the transition from higher biomass and rates to lower biomass and rates occurred in 1995, and was largely due to the exceptionally stormy summer that year.

Taken at face value, the direct N_2-fixation rate estimates for the North Atlantic reported by Carpenter and McCarthy (1975) and Carpenter and Price (1977) suggest that N_2-fixation rates in the 1970s were much lower than they were in the early 1990s. The combination of these data with more recent rate estimates and the model results suggests a general pattern of lower *Trichodesmium* biomass and N_2-fixation rates in the 1970s, increased rates in the late 1980s and early 1990s, followed by lower rates again in 1995–1997. This general pattern of variability is roughly consistent with well-known, decadal-scale variations in North Atlantic Climate, i.e., the North Atlantic Oscillation (NAO). The NAO index, derived from sea-level pressure anomalies across the North Atlantic, shifted from a predominantly negative pattern in the 1960s and early 1970s to a predominantly positive pattern in the late 1980s and early 1990s (Hurrel, 1995). The index then shifted

abruptly back again to strong negative values in 1995 (Halpert and Bell, 1997). At Bermuda, negative indices are associated with increased storm frequency and generally colder and wetter winters, whereas positive indices are associated with reduced storm frequencies and generally milder winters. If, indeed, *Trichodesmium* populations are sensitive to the depth and duration of winter mixing as the model results suggest, then one might expect significantly lower rates and biomasses in the 1960s and 1970s, higher rates in the late 1980s and early 1990s, and lower rates again in 1995 in response to the NAO. Although negative indices are not generally associated with increased storm frequency in summer, there could be a link between the unusually stormy summer of 1995 and the return to the strong negative phase of the NAO. Thus, the abrupt decline in *Trichodesmium* generated by the model in 1995 also may be related to the NAO.

This apparent interannual variability in *Trichodesmium* biomass and N_2-fixation rates also coincides with a recent analysis of temperature anomalies at BATS (Bates, 2001); i.e., the low biomasses and rates generated by the model in 1995 and 1996 (Fig. 4) coincide with negative (cold) temperature anomalies and the high biomass and rates generated by the model in 1989–1990 and 1994 coincide with positive (warm) temperature anomalies. These temperature anomalies also appear to coincide with variations in N_2-fixation in the observations, i.e., the observations of Orcutt et al. (2001) in 1995 correspond with the coldest negative temperature anomaly in the record whereas the 1990 observations of Carpenter and Romans (1991) coincide with a strong warm anomaly for the entire year. If the hypothesized link between *Trichodesmium* abundance and the NAO is correct, it suggests that the N_2-fixation rates in 1990 should have been higher. In addition, the data from 1970s collected by Carpenter and McCarthy (1975) and Carpenter and Price (1977) coincide with a period of cold anomaly much greater than 1995, which suggests that rates of N_2-fixation may have been particularly low at that time. Bates (2001) shows that these temperature anomalies statistically correlate with the NAO. Bates also shows that the integrated primary production rates are higher and mixed-layer depth is deeper during cold anomalies and vice versa. Thus, it appears that interannual variability associated with NAO may, indeed, have significant impact on both phytoplankton production and N_2-fixation at BATS, and that it may be an important factor in determining the outcome of competitive interactions between phytoplankton and *Trichodesmium*.

3.2.2. Modeled vs. observed DIC and export fluxes

Figs. 5 and 6 compare the model-predicted DIC concentrations and export fluxes at 300 m with the BATS observations. In S1, where the sinking rate and *Trichodesmium* mortality were tuned to fit the observed DIC and primary production, the model reproduces the DIC concentrations quite well (Fig. 5, middle panel), but consistently overestimates the 300-m trap fluxes by more than a factor of 4 (Fig. 6). This happens because the high N_2-fixation rates that are required to drawdown the DIC to the observed levels (Fig. 5) must be approximately balanced by increased export flux of particulate nitrogen (Fig. 6). If the input of N due to N_2-fixation is not balanced by export, DIN accumulates within the model domain which, in turn, leads to increased phytoplankton biomass and production rates that are too high. In order to achieve this balance the sinking rate of detritus has to be increased to 12 m d^{-1} (Table 1). Although the resulting export fluxes are significantly higher than the measured values, there is substantial uncertainty in the trap flux measurements, i.e., perhaps as much as a factor of 2–3 (Buesseler, 1992; Michaels et al., 1994). Thus it is possible that the S1 export fluxes are within the error variability of the sediment trap

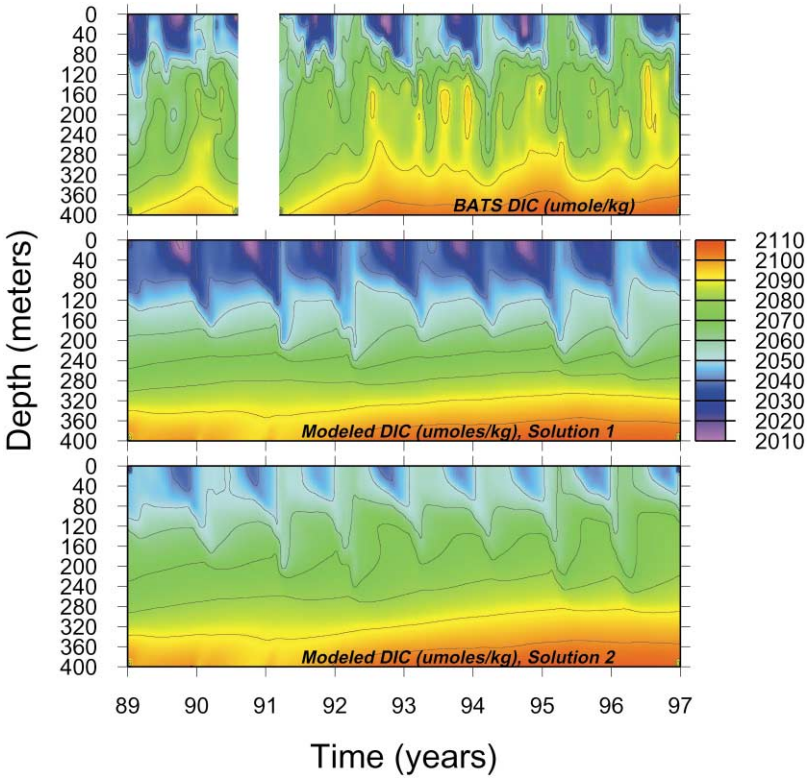

Fig. 5. Comparison of observed DIC concentrations at BATS (top panel) with model-estimated DIC concentrations from S1 (middle panel) and S2 (bottom panel).

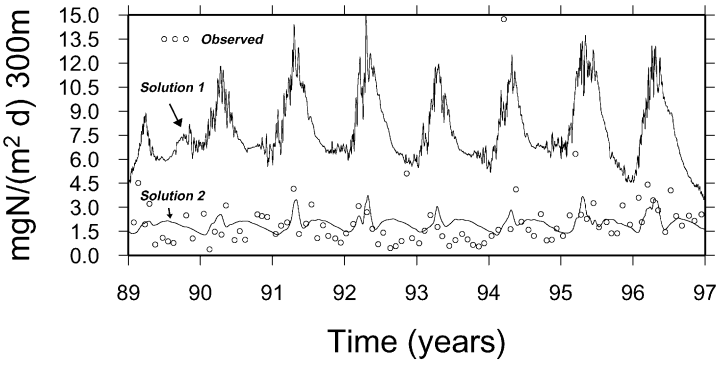

Fig. 6. Comparison between the observed 300-m sediment trap nitrogen fluxes and the model-predicted 300 m nitrogen (detritus) fluxes for S1 and S2.

measurements. In addition note that the seasonal pattern in the S1 model-generated 300 m fluxes is basically similar to the pattern in the measured fluxes, especially after 1991.

In contrast, in S2, where the model was tuned to fit the trap fluxes and primary production, the magnitude of the fluxes is approximately correct (Fig. 6), but the DIC concentrations near the

surface in mid-summer are generally too high by 20–30 μmol kg^{-1} (Fig. 5, bottom panel). This happens because the nitrogen fixation rate has to be lowered enough to prevent accumulation of nitrogen, which results in insufficient drawdown of DIC. Unlike the trap fluxes, the DIC measurements are fairly precise (i.e., the measured values are accurate to within $\pm$ 0.4 μmol kg^{-1}) so the difference between the observed summer values and the S2 DIC concentrations cannot be attributed to measurement error. Note that although the magnitude of the 300 m fluxes is approximately correct in S2, the observed seasonal variability is not well reproduced by the model (Fig. 6).

In S1 the model reproduces the interannual variability in DIC concentrations reasonably well, i.e., the model predicts more drawdown in 1989 and 1992–1994, and less drawdown in 1991 and 1995–1996 as observed (Fig. 5, top and middle panels). In S1 the interannual variability in DIC drawdown appears to be driven primarily by interannual variability in the summertime N_2-fixation rate. For example, 1995–1996 are relatively low *Trichodesmium* years, which results in less DIC drawdown whereas 1989–1994 are relatively high *Trichodesmium* years, which results in more DIC drawdown. Thus, according to the model the relatively weak drawdown of DIC that was observed in 1995–1996 compared to previous years was due to reduced N_2-fixation which was, in turn, the result of exceptionally stormy weather in 1995 and to a lesser extent in 1996. If the hypothesized link between *Trichodesmium* abundance and the NAO is correct, it suggests that negative NAO index periods should be associated with less DIC drawdown at BATS and vice versa.

The model also reproduces the seasonal cycle and the timing of the summertime drawdown of DIC quite accurately in S1. The minimum DIC concentrations develop when the N_2-fixation rates are at their peak values and persist as the rates begin to decline (compare Figs. 4 and 5). The tight correspondence between the model-predicted and observed DIC variability at both seasonal and interannual timescales in S1, which appears to be driven by variability in rates of N_2-fixation, strongly suggests that high N_2-fixation is, indeed, responsible for the anomalous DIC drawdown that is observed in late summer at BATS as suggested by Michaels et al. (1994), Bates et al. (1996) and Marchal et al. (1996).

The most obvious difference between the modeled DIC concentrations and the observations is that there is much more high-frequency (weekly/monthly) variability in the observations (Fig. 5). This difference exists in spite of the fact that the model is forced with high-resolution meteorological data at the surface and observed DIC concentrations at the bottom boundary, and is likely due to the absence of mesoscale eddy variability in the model. Perhaps the most significant difference between the model results and the observations is that the model tends to underestimate DIC concentrations at mid-depth (approximately 120–240 m, Fig. 5). In S1 the model also consistently underestimates the surface DIC concentrations during deep-mixing events in late winter/early spring by 10–20 μmol kg^{-1} (Fig. 5). As discussed above, when estimating N_2-fixation rates from DIC drawdown it is important to reproduce the initial late winter/early spring DIC concentrations as accurately as possible because this pool largely determines the total amount of nitrogen required from N_2-fixation. Thus, underestimation of the initial DIC pool suggests that the S1 N_2-fixation rates also have been underestimated. The discrepancy at the surface in S1 appears to be the result of the low DIC values in the interior, i.e., deep mixing in winter does not pull enough DIC up to the surface because the DIC concentrations are too low in the upper thermocline.

The low DIC values in the upper thermocline in the solutions may be due to the absence of isopycnal and mesoscale mixing processes and/or horizontal advection of DIC in this 1-D model.

As discussed above, an attempt has been made to parameterize the effect of some of these processes with increased turbulent diffusion, but this parameterization may not be sufficient. Alternatively, the low DIC concentrations in the interior could be due to some deficiency in the biological model. For example, there may be insufficient remineralization of carbon from sinking particulate material in this mid-depth range. Another possibility is that it is due to the absence of refractory forms of DON/DOC in the model. At BATS, remineralization of DOC in the subsurface during summer from DOC produced during the late winter/early spring bloom is a significant contributor to DIC in this depth range (Carlson et al., 1994). In the model, the labile DON/DOC produced during the bloom cannot persist until summer.

3.2.3. Modeled vs. observed production and f-ratio

Fig. 7 shows the interannual variability in the observed and modeled particulate phytoplankton production and the 300-m *f*-ratios for S1 and S2. Both solutions capture much of the observed seasonal and interannual variability in primary production, but there are some obvious discrepancies between the model results and the observations, and there are some significant differences

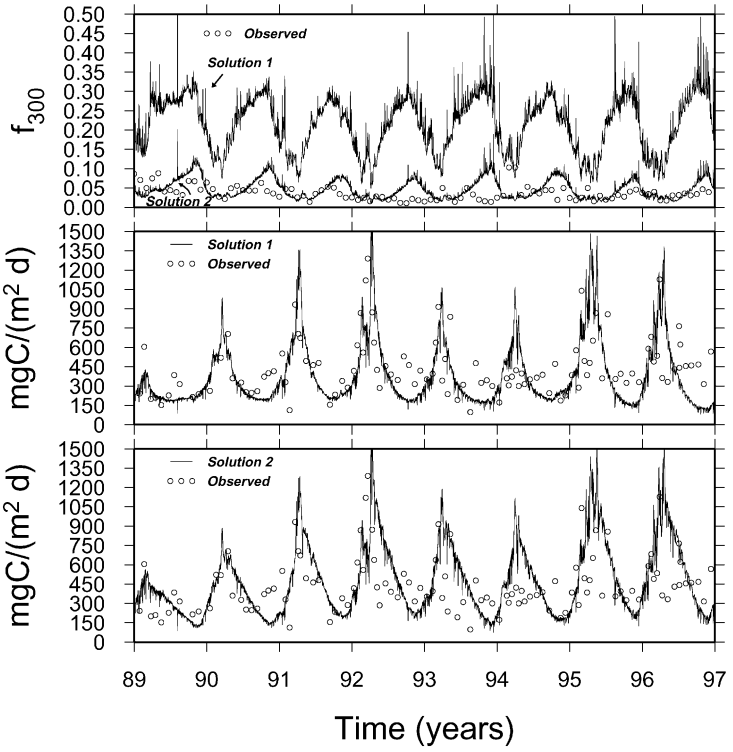

Fig. 7. Comparison between the vertically integrated BATS ^{14}C particulate primary production rates and vertically integrated particulate phytoplankton production predicted by the model for S2 (bottom panel) and S1 (middle panel). The model particulate production rates were calculated assuming a phytoplankton C : N ratio of 10 (see Section 2.3 for details). The top panel compares the model-estimated 300-m *f*-ratios (f_{300}) for S1 and S2 (calculated by dividing the downward 300-m nitrogen flux by the primary particulate nitrogen production) with the observed 300-m *f*-ratios (calculated by dividing the 300-m sediment trap carbon fluxes by integrated ^{14}C primary production rates).

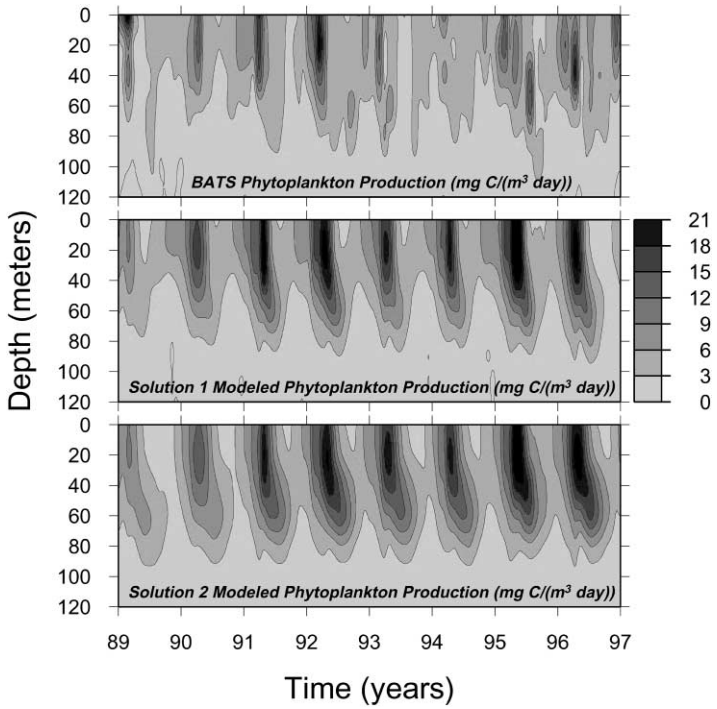

Fig. 8. Comparison of the observed subsurface particulate primary production with the S2-estimated (bottom panel), S1-estimated (middle panel) values. Again, the modeled rates were calculated assuming a phytoplankton C : N ratio of 10 (see Section 2.3 for details).

between S1 and S2. As observed at BATS, the productivity peaks are associated with detrainment of the mixed layer in the spring and they are fueled by the nutrient supply provided by deep winter mixing. The productivity minima occur during summer when the water column is stratified and nutrient supplies are reduced (compare Figs. 3A and 7). Note that the model produces stronger production peaks in 1991, 1992, 1995 and 1996 as observed, and lesser peaks in 1989, 1990, 1993 and 1994 as observed. The most obvious discrepancy between the observations and the model solutions occurs in 1994 when the model produces a distinct spring production peak where none was observed (Fig. 7). This discrepancy may be due to the fact that in the model the mixed layer penetrated deeper than observed in winter/early spring of 1994. As a result the model bloomed whereas in reality no distinct spring bloom occurred.

Contrasting solutions 1 and 2 reveals a distinct difference in the seasonal production patterns: In the low N_2-fixation case, S2, the production rates tend to remain higher after the late winter/early spring production peak. The reason for this is subtly revealed in Fig. 8, which shows the observed and modeled subsurface production rates. The integrated rates tend to remain higher after the peak in S2 because this solution produces slightly higher rates at depth following the spring maximum. This happens because slower sinking rates promote more recycling and production in the 40–80 m depth range. Note, however, that both solutions sometimes significantly underestimate the

Table 4
Average annual *f*-ratios[a] computed from model solutions 1 and 2 and from direct BATS observations for each year and means for 1989–1994 and 1995–1996

Year	f_{300}^{DIN}	f_{300}^{DON}	f^{NFIX}	f_{300}^{TOT}	f_{300}^{DETR}	f_{300}^{BATS}
	Solution 1 (solution 2)					
1989	5.46 (5.29)	− 0.0033 (− 0.0063)	24.88 (3.01)	30.34 (8.30)	− 17.77 (− 5.25)	**−5.64**
1990	3.62 (3.67)	− 0.0033 (− 0.0053)	15.76 (2.24)	19.38 (5.90)	− 15.58 (− 4.21)	**−4.21**
1991	2.81 (2.85)	− 0.0041 (− 0.0052)	11.97 (1.50)	14.78 (4.35)	− 14.80 (− 3.50)	**−3.31**
1992	3.13 (2.77)	− 0.0057 (− 0.0060)	9.00 (0.70)	12.13 (3.46)	− 14.21 (− 3.08)	**−1.99**
1993	3.06 (2.64)	− 0.0036 (− 0.0048)	14.41 (0.97)	17.47 (3.60)	− 16.08 (− 3.56)	**−2.33**
1994	2.42 (2.37)	− 0.0033 (− 0.0048)	15.26 (1.34)	17.68 (3.71)	− 15.46 (− 3.76)	**−5.00**
1995	2.03 (1.80)	− 0.0048 (− 0.0051)	5.82 (0.30)	7.85 (2.10)	− 13.82 (− 2.99)	**−2.72**
1996	3.19 (2.17)	− 0.0068 (− 0.0065)	5.46 (0.11)	8.64 (2.27)	− 14.96 (− 3.14)	**−3.06**
1989–1994	3.42 (3.26)	− 0.0039 (− 0.0054)	15.21 (1.63)	18.63 (4.89)	− 15.65 (− 3.89)	**−3.75**
1995–1996	2.61 (1.98)	− 0.0058 (− 0.0058)	5.64 (0.21)	8.24 (2.18)	− 14.39 (− 3.06)	**−2.89**

[a]Expressed as % of particulate phytoplankton production.

integrated rates in late summer and fall (Fig. 7). This problem is probably related to the application of a seasonally constant sinking rate which results in too much export and too little recycling when the water column is strongly stratified. Fig. 8 also shows a general lack of higher frequency variability, as discussed above.

The top panel of Fig. 7 shows the 300-m *f*-ratios (f_{300}) for both S1 and S2, which are calculated by dividing the model-generated 300-m export flux by the model-generated, water-column (integrated) particulate production. For comparison f_{300}, calculated from the BATS ^{14}C-measured production rate and 300-m sediment trap carbon fluxes, is also plotted. The magnitude of f_{300} in S2 agrees reasonably well with the observed values because S2 was tuned to fit the observed 300-m fluxes and the observed rates of primary production. The most significant discrepancies occur consistently in late summer/early fall, when the model tends to underestimate the integrated primary production (Fig. 7, bottom panel). This, in turn, results in *f*-ratios that are too high. Annual *f*-ratios in S2 vary between 2.1 and 8.3% compared to a range of 1.99–5.64% calculated from the observations (Table 4). In contrast, f_{300} in S1 is much higher than the values calculated from the BATS data, varying between 7.9 and 30% (Table 4).

When the individual sources of new nitrogen are considered (Table 4) it can be seen that the differences in export between S1 and S2 are balanced almost entirely by differences in N_2-fixation. Both solutions have similar DIN influxes and negligibly small DON effluxes. In the case of S2 the nitrogen contributions from N_2-fixation and upward DIN flux are roughly comparable, which is consistent with the calculations of Capone et al. (1997) for oligotrophic tropical waters. In contrast, in S1 the contributions of nitrogen from N_2-fixation are generally 2–5 times greater than those from the upward DIN flux.

3.2.4. The DIN and DON distributions

Although the model was not specifically tuned to reproduce the observed DIN concentrations, Fig. 9 shows that both S1 and S2 produce reasonable results. As observed, the DIN concentrations are generally near zero at the surface during summer in S1 and S2, and the nutricline in both model solutions is in approximately the right place. The model also produces slight increases in DIN concentrations at the surface in the late winter/early spring during deep-mixing events as observed. Thus, tuning the model to give the correct production rates and DIC concentrations or export fluxes constrains DIN concentrations fairly well, and it suggests that using a C : N ratio of 10 is an appropriate choice. The latter conclusion is supported by the fact that when the model is run with C : N = 6.625 (Redfield) and tuned to the observed production rates and DIC concentrations, the agreement between the observed and modeled DIN concentrations is not as good (solution not shown). Specifically, with Redfield C : N the model tends to have too much DIN in the mixed layer and the nutricline is too shallow.

As with DIC and subsurface production, the most obvious difference between the modeled DIN concentrations and the observations is that there is much more high-frequency (weekly/monthly) variability in the observations (Fig. 9). A comparison of the top panels in Figs. 5 and 9 reveals that the high-frequency variability in DIN and DIC concentrations is roughly coherent, again

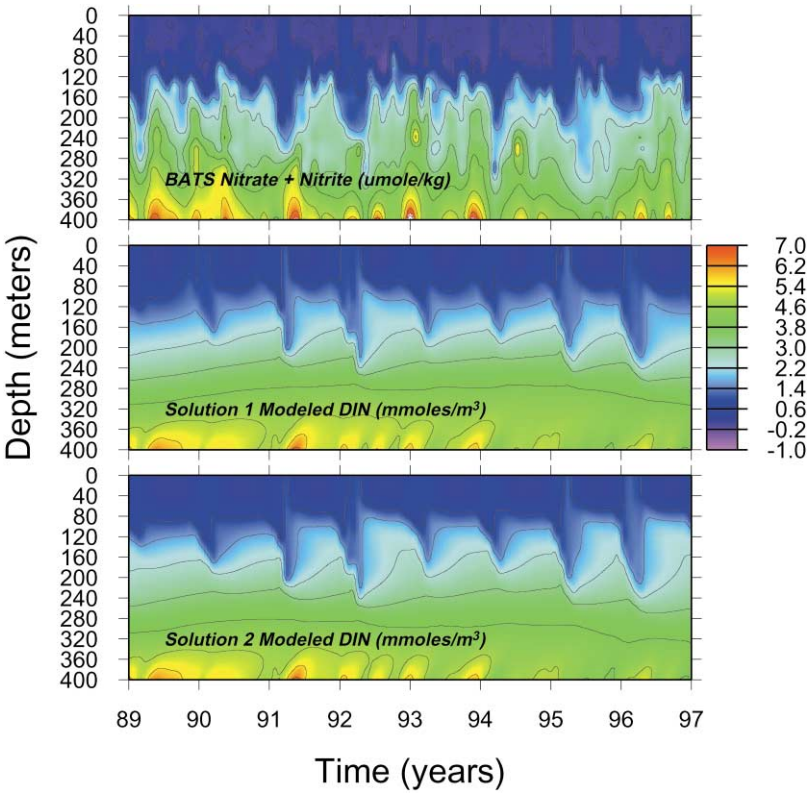

Fig. 9. As in Fig. 5 for model-estimated DIN and BATS nitrate + nitrite.

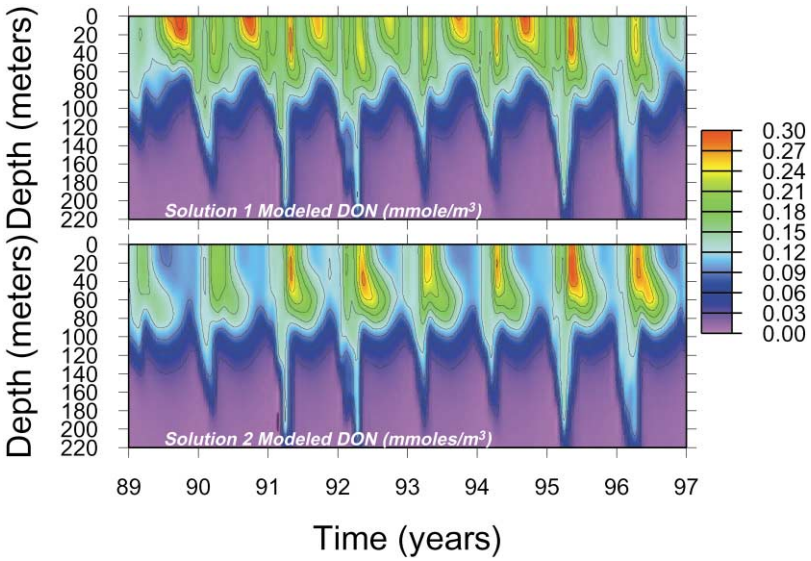

Fig. 10. Comparison between labile DON concentrations generated by S2 (bottom panel) and S1 (top panel).

suggesting that it is driven by horizontal, mesoscale variability (e.g., the passage of eddies, McGillicuddy et al., 1998; Siegel et al., 1999) not represented in the model.

Fig. 10 shows that the labile DON concentrations predicted by the model are almost inversely related to DIN concentrations in both S1 and S2; i.e., below the nutricline DON drops rapidly to 0, and the highest concentrations (0.3 mmol m^{-3}) are found in the euphotic zone above the nutricline. In both solutions, DON maxima are produced during the late winter/early spring productivity maximum. This happens because DON production is proportional to primary production; i.e., following Bronk et al. (1994), Glibert and Bronk (1994) and Capone et al. (1994) 30% of both phytoplankton and *Trichodesmium* production is shunted directly to DON. The most obvious difference between S1 and S2 is the consistent development of a second DON maximum in S1 in late summer and fall in the upper 40 m of the water column. This distinct secondary maximum is entirely absent in S2. The concentrations associated with this maximum vary between 0.12 and 0.30 mmol m^{-3}. A comparison of Figs. 10, 5 and 4 reveals that this feature develops exactly at the same time as the N_2-fixation maximum and the DIC minimum and thus appears to be associated with *Trichodesmium* N_2-fixation; i.e., the secondary maximum in late summer and fall in S1 appears to be the result of direct exudation of DON and/or indirect production of DON from other ecosystem compartments fueled by nitrogen derived from N_2-fixation. Although it is not explicitly modeled, the presence of a labile DOC maximum with concentrations between 1.2 and 3 μmol kg^{-1} (using $C:N = 10$) also is implied.

Although there are relatively few DON measurements in the Atlantic Ocean, typical open-ocean concentrations are in the range of 3–7 mmol m^{-3} with only small variations with depth (Sharp, 1983; Hansell and Carlson, 2001). Presumably, most of this pool is refractory. More labile

components of the DON pool typically vary between 0.05 and 1.0 mmol m^{-3} (Sharp, 1983, see his Table 3). Thus, the 0.12–0.30 mmol m^{-3} range of concentrations produced by the model, which represent labile forms of DON, agree quite well with the known open-ocean ranges. The second increase in DON in late summer/early fall in S1 is of particular interest because if, indeed, *Trichodesmium* production at BATS is high enough to drawdown DIC concentrations to the observed levels, and the DON release rates are as high as those reported by Glibert and Bronk (1994) and Capone et al. (1994), then there should be late summer/early fall maxima in DON and DOC concentrations at BATS. Recent measurements, however, do not show evidence of this DON anomaly at BATS in late summer/early fall (Hansell and Carlson, 2001). In this regard, though, it should be noted that the DON anomaly generated by the model (0.12–0.30 mmol m^{-3}) is close to the precision limit of the DON analysis method so it is conceivable that there is a signal that is masked by the noise in the measurement. The expected DOC anomaly (1.2–3 μmol kg^{-1}) however, would be detectable (Hansell and Carlson, pers. comm.), but this anomaly is not clearly observed either. Measurable DON anomalies have been observed in stratified regions of the southwestern Equatorial Atlantic (Vidal et al., 1999) and Pacific Oceans (Karl et al., 1995, 1997; Hansell and Feely, submitted) in association with high *Trichodesmium* concentrations.

3.3. Model sensitivity

In this section results are presented that demonstrate the sensitivity of the model-estimated N_2-fixation rates to selected parameters. These include two key physical and chemical parameters — diffusion (K_w) and the C : N ratio — and four biological parameters that govern *Trichodesmium* growth and biomass — the initial biomass, the maximum growth rate (μ_T), the DON partitioning parameter (α) and the half-saturation constant for DIN uptake (TK_s). Sensitivity was quantified by modifying the parameters and then retuning the model to fit the observed DIC concentrations and production rates (solution 1) and the observed sediment-trap fluxes and production rates (solution 2). The resulting annually integrated N_2-fixation rates are compared to the mainrun S1 and S2 solutions for 1994 in Table 5. The year 1994 was chosen for comparison because it is a relatively high N_2-fixation rate year that is far enough in the run to be minimally affected by transient model responses. The comparison is made *after* retuning because the objective is to determine the impact of changing parameter values on the model-estimated N_2-fixation rates that are derived by tuning; i.e., the question is, how different would the estimated rates be if different, but still reasonable, parameter values had been used instead. For a general assessment of the response of these kinds of models to changes in the biological and physical parameters see Fasham et al. (1990) and McCreary et al. (1996).

Table 5 shows that when the model is run with turbulent diffusivities from Ledwell et al. (1998) the model-predicted N_2-fixation rates are decreased by 33% in S1 and increased by more than 300% in S2. The rates decrease in S1 because, as discussed above, with the lower K_w the model substantially underestimates the DIC concentrations in the upper thermocline. This, in turn, lowers the initial late winter/early spring DIC pool, which largely determines the model-predicted annual rate. The lower DIC concentrations in the upper thermocline may also significantly reduce the DIC flux from the interior into the stratified surface layer during summer and DIC entrainment in the fall/early winter, which would also reduce the model-predicted N_2-fixation rates. In contrast, the rates in S2 are dramatically increased with the lower K_w because N_2-fixation has to be increased in

Table 5
Sensitivity of the model-estimated N_2-fixation rates to diffusion, C:N ratio, initial conditions and the *Trichodesmium* growth parameters

Parameter (mainrun/modified)	S1 main/modified	S2 main/modified
	(mmol N m^2 yr^{-1})	
K_w (0.0001/0.000017 m^2 s^{-1})[a]	201/135 (− 33%)	18/73 (+ 305%)
C:N ratio (10/6.625 dimensionless)[b]	201/218 (+ 8.5%)	18/26 (+ 44%)
Initial [*Tricho*] (0.005/0.01 μmol m^{-3})	201/200 (− 0.5%)	18/18.4 (+ 2.2%)
μ_T (0.17/0.14 d^{-1})[c]	201/238 (+ 18.4%)	18/33 (+ 83.3%)
α (0.70/0.90 dimensionless)	201/213 (+ 6.0%)	18/1.2 (− 93.3%)
TK_s (0.5/6.7 mmol m^{-3})[d]	201/276 (+ 37.3%)	18/20 (+ 11.1%)

[a] $K_w = 0.000017$ m^2 s^{-1} from Ledwell et al. (1998).
[b] C:N = 6.625 = 106/16 from Redfield et al. (1963).
[c] $\mu_T = 0.14$ d^{-1} is equal to a doubling time of 5 d, from Capone et al. (1997).
[d] $TK_s = 6.7$ mmol m^{-3} from McCarthy and Carpenter (1975).

order to maintain production rates at the observed levels; i.e., new nitrogen has to be supplied from the atmosphere to compensate for the reduced new nitrogen influx from below.

In both S1 and S2, decreasing the C:N ratio from 10 to 6.625 significantly increases the estimated rates. As discussed above, this happens in S1 because lowering the C:N ratio of the particulate matter increases the amount of N_2-fixation required to lower the DIC concentrations to the observed levels and increases the nitrogen export flux that is required to remove this DIC from the model domain. The effect of lowering the C:N ratio in S2 is even more pronounced than it is in S1. This is surprising because changing the C:N ratio has no direct impact on the model-predicted nitrogen export flux at 300 m. It does, however, decrease the production rate predicted by the model because the C:N ratio is also used to convert the model-estimated nitrogen uptake to carbon uptake. Thus, N_2-fixation has to be increased in S2 when the C:N ratio is lowered in order to maintain the observed production rates.

Table 5 shows that the model is not very sensitive to the initial *Trichodesmium* biomass. However, the estimated N_2-fixation rates are sensitive to the other three *Trichodesmium* parameters. Lowering the growth rate, μ_T, to a value equivalent to a doubling time of 5 d (which is the low end of the range of growth rates summarized in Capone et al. (1997)) significantly increases the model-estimated N_2-fixation rates in S1 and S2 (Table 5). Increasing the half-saturation constant for DIN uptake, TK_s, to 6.7 mmol m^{-3} (following McCarthy and Carpenter, 1975), also significantly increases the rates in S1 and S2. Both of these effects are counterintuitive. Suffice it so say that if the maximum growth rate of *Trichodesmium* is significantly lower than 0.17 d^{-1} and/or their affinity for DIN is comparable to that reported by McCarthy and Carpenter (1975) then the estimated rates will be significantly higher in both solutions.

Decreasing α to 0.90 (10% of primary production released directly to DON) has relatively little effect upon the S1-estimated N_2-fixation rates (6% increase). However, it dramatically

lowers the S2-estimated rates (93.3% decrease) (Table 5). The latter happens because the increased α significantly increases particulate primary production which, in turn, reduces the amount of N_2-fixation required to reproduce the observed production rates and export fluxes. In fact, with $\alpha = 0.90$ *Trichodesmium* is nearly extinct by the end of the S2 run (not shown). Although the S1-estimated N_2-fixation rates are not altered very much with $\alpha = 0.90$, this change does have a significant effect on the S1-estimated DON concentrations; i.e., it decreases the DON concentrations associated with the spring phytoplankton bloom and nearly eliminates the late summer/early fall anomaly associated with the *Trichodesmium* bloom (not shown). Thus, the strength of model-predicted DON anomaly discussed above is critically dependent upon the specification of α, and the presence of a significant signal requires relatively high fractional DON release from *Trichodesmium*.

In summary, the effect of changing these parameters is, in some cases, substantial and the effects tend to be much more pronounced in S2 (Table 5). However, regardless of the parameter values, the estimated rates are always much greater in S1 than in S2, and all of the S1 estimates in Table 5 are consistent with the high geochemical rates.

4. Summary and conclusions

This paper describes an attempt to model the effect of N_2-fixation on nitrogen and carbon fluxes at BATS using a relatively simple one-dimensional, biogeochemical model with an explicit representation of *Trichodesmium* biomass and N_2-fixation. The formulation assumes that *Trichodesmium* production is limited primarily by its own slow intrinsic growth rate and the availability of light. The model reproduces the general characteristics of the observed *Trichodesmium* biomass distributions and seasonal N_2-fixation cycles at BATS; i.e., the biomass of *Trichodesmium* is restricted to the upper 50 m of the water column and varies seasonally with peak biomasses and rates in late summer/early fall. This alone strongly suggests that the model includes the essential limiting factors which control *Trichodesmium* growth and abundance at BATS.

However, two potentially important limiting nutrients are not represented in this model: phosphorus and iron. Phosphorus must be supplied to have a significant net N_2-fixation-driven carbon export because export requires the formation of particulate organic matter which, in turn, requires phosphorus. A variety of hypotheses have been proposed for delivering phosphorus from depth to the near-surface ocean where *Trichodesmium* grows, e.g., "phosphorus mining" (Karl et al., 1992). Regardless of the means by which it is obtained, the fact remains that high rates of N_2-fixation have been measured in many different ocean regions in the absence of measurable phosphate, and phosphorus addition assays that have been performed with *Trichodesmium* have not consistently revealed significant phosphorus limitation (Hood et al., 2000). Thus, it may not be necessary to include explicit representation of phosphorus in models aimed at predicting seasonal and interannual variability. However, it will almost certainly be necessary to include both nitrogen and phosphorus in models that attempt to predict longer term changes in N_2-fixation (e.g., Tyrrell, 1999).

Because of the presumed high iron requirement of the nitrogenase enzyme and the general global correspondence between regions of high iron deposition and high N_2-fixation it has generally been assumed that N_2-fixation is subject to Fe-limitation (Capone et al., 1997). Moreover, Orcutt

et al. (2001) report a general correspondence between interannual variability in *Trichodesmium* abundance, rates of N_2-fixation, and atmospheric Fe deposition at BATS over the time period they sampled (1995–1997), and they speculate that Fe-limitation is responsible. Thus, *Trichodesmium* growth and N_2-fixation at BATS may be constrained by Fe. Future development of the model presented here will be aimed at including some form of Fe-limitation. It should be emphasized, however that the evidence for Fe-limitation to date is largely circumstantial (Hood et al., submitted).

It is also important to keep in mind that this model does not include some, potentially important, ecological characteristics of *Trichodesmium* that could impact the N_2-fixation rate estimates. For example, it is believed that *Trichodesmium* controls its bouyancy by accumulating carbohydrate "ballast" and respiring this ballast at depth (Karl et al., 1992; Letelier and Karl, 1998). This process could result in a significant downward flux of carbon that is not accounted for in the model. There is also some evidence that *Trichodesmium* (and other organisms which control bouyancy) tend to accumulate at the base of the mixed layer which could affect the model-estimated rates (Letelier, 1994). Thus, the simple model of *Trichodesmium* presented here should be considered as a starting point. Clearly, future efforts also should include some of these more complex aspects of *Trichodesmium's* behavior and physiology to determine how this impacts the estimated rates.

The solutions presented in this paper suggest that there is strong interannual variability in *Trichodesmium* biomass and N_2-fixation at BATS which is related to the depth and frequency of wind mixing through its impact on the availability of light; i.e., there appears to be an inverse relationship between the depth of winter mixing and the strength of the late summer/early fall *Trichodesmium* bloom. When winter mixing is relatively deep and the phytoplankton bloom is strong (both of which reduce the availability of light in the mixed layer) *Trichodesmium* does less well and vice versa. In addition, there appears to be a significant effect of summertime storminess. In particular, during the summer of 1995, which had the highest frequency of summer storms and hurricanes in over a decade, the model suggests that the *Trichodesmium* population was strongly affected. These results are consistent with observations that show that *Trichodesmium* populations are very sensitive to wind-induced mixing (Capone et al., 1997; D.G. Capone, personal observations); i.e., blooms tend to form under stratified conditions that develop during periods of quiescent weather, and they dissipate rapidly when wind mixing increases. Rarely, if ever, are *Trichodesmium* blooms observed in windy, well-mixed conditions. In the model the relationship between mixing/stratification and absence/presence of *Trichodesmium* appears to involve competitive interactions with phytoplankton; i.e., *Trichodesmium* flourishes only under stratified, high-light, DIN-depleted conditions that maximize the growth rate of *Trichodesmium* and restrict the growth of phytoplankton. Otherwise, *Trichodesmium* cannot compete due to its slow intrinsic rate of growth.

Two solutions are presented, one where the N_2-fixation rate is tuned to reproduce the observed DIC concentrations and primary production (S1), and the other where it is tuned to reproduce the observed 300-m trap fluxes and primary production (S2). Although these two solutions are similar in many respects they give dramatically different estimates of *Trichodesmium* biomass and N_2-fixation rates at BATS; i.e., S1 generates very high biomasses and annual rates that are consistent with the geochemical estimates of Michaels et al. (1996) and the direct rate estimates of Carpenter and Romans (1991) for the Sargasso Sea, whereas S2 generates much lower biomasses and rates, which are generally more consistent with direct rate measurements for this region from the 1970s

(e.g., Carpenter and McCarthy, 1975; Carpenter and Price, 1977). Although both solutions reproduce observed rates of primary production and DIN concentrations reasonably well, two clear inconsistencies arise: S1 generates nitrogen export fluxes that are more than 4 times higher than the measured BATS trap fluxes, and S2 generates near-surface DIC concentrations in late summer/early fall which are 20–30 μmol kg^{-1} higher than observed. Thus, in order to reproduce the DIC concentrations near the surface it is necessary to export far more nitrogen (and carbon) than is observed, and in order to reproduce the measured 300-m sediment trap nitrogen fluxes it is necessary to substantially overestimate the near-surface DIC.

This basic dilemma was first recognized by Michaels et al. (1994) as an imbalance in the carbon budget at BATS, and they suggested that it can be explained by failure to account for horizontal advection of carbon or by inaccuracies in the fluxes of sinking particles as measured using sediment traps. They also suggested that the depletion of DIC in late summer/early fall that occurs in the absence of measurable nutrients could be driven by nitrogen fixation. The results presented in this paper do not resolve the carbon budget dilemma. Even if it turns out that the N_2-fixation is responsible for the depletion of DIC at BATS, the imbalance in the carbon (and nitrogen) budgets remains. Moreover, the potential role of horizontal advection is not addressed here at all. However, the model does show conclusively that the N_2-fixation rates implied by the DIC drawdown are consistent with observed excess nitrate concentrations (N*) in the upper thermocline at BATS (Michaels et al., 1996). The model results also highlight two additional pieces of evidence that support the idea that the N_2-fixation is responsible for the late summer/early fall drawdown of DIC. First, both the model and the direct observations of Orcutt et al. (2001) show that the highest rates of N_2-fixation at BATS are coincident with the anomalous late summer/early fall DIC drawdown. And second, the model reproduces the interannual variability in the late summer/early fall DIC drawdown, which arises in the model as a result of interannual variability in N_2-fixation rate. There are, however, conflicting results as well, i.e., S1 predicts DON and DOC anomalies in late summer/early fall at BATS which are not observed.

There is insufficient data to determine conclusively whether or not the interannual variability in N_2-fixation generated by the model is correct. However, the model suggests that *Trichodesmium* biomass and N_2-fixation rates were substantially higher from 1989 to 1994 compared to 1995 to 1996, and this result is consistent with the observations of Carpenter and Romans (1991) and Orcutt et al. (2001) and the observed variations in near-surface DIC concentrations at BATS. If this decadal-scale change in the rates actually happened, it could help to explain discrepancies between geochemical N_2-fixation rate estimates and more recent direct rate estimates because the former integrate the effects of rates over the previous 5–10 yr. It also may help to explain the large differences in the direct rate measurements that have been made in the Sargasso Sea over the last 30 yr; i.e., the rates may, indeed, have been much lower in the 1970s, higher in the late 1980s and early 1990s and then lower again in the late 1990s. If *Trichodesmium* populations in the Sargasso Sea are as sensitive to the depth of winter mixing and storm frequency as the model (and direct observations) suggest, it is likely that natural decadal-scale variability in the North Atlantic ocean (i.e., the North Atlantic Oscillation) has caused major changes in the abundance of *Trichodesmium* and N_2-fixation rates. Thus, it is possible that at least some of the discrepancies between various rate estimates that have been made over the years in the Sargasso Sea are simply the result of undersampling a population of organisms that varies substantially on timescales of 1–10 yr in response to natural modes of atmospheric variability.

Acknowledgements

The authors thank Frank Millero for providing the original code that was used to develop the CO_2 chemistry model and Kevin Maillet for implementing it. We thank Fred Lipschultz, Ed Carpenter, Dennis Hansell, Craig Carlson and Victoria Coles for discussing various aspects of this work. We also thank Ricardo Letelier and another anonymous referee for their careful and helpful reviews. Special thanks go to all of the personnel that have been involved in the collection, processing and analysis of the Bermuda Atlantic Time Series station data over the past decade. The original biogeochemical model development was funded by an NASA grant (NAGS-3619 to R. Fine and D. Olson) with additional support from NSF (grants OCE94-13222 and OCE92-07237 to R. Fine). The implementation of the model at BATS and the analysis described here was funded by an NSF grant (OCE96-28888) to R. Hood and NASA SMP grants to R. Hood (NAG5-6387) and D. Capone (USC grant number pending). Capone's work on *Trichodesmium* has been largely supported by NSF grant OCE96-33510.

References

Altabet, M.A., 1988. Variations in nitrogen and isotopic composition between sinking and suspended particles: implications for nitrogen cycling and particle transformation in the open ocean. Deep-Sea Research 35, 535–554.

Antia, N.J., Harrison, P.J., Oliveira, L., 1991. The role of dissolved organic nitrogen in phytoplankton nutrition, cell biology and ecology. Phycologia 30, 1–89.

Bates, N.R., 2001. Interannual variability of oceanic CO_2 and biogeochemical properties in the Western North Atlantic subtropical gyre. Deep-Sea Research II 48, 1507–1528.

Bates, N.R., Michaels, A.F., Knap, A.H., 1996. Seasonal and interannual variability of oceanic carbon dioxide species at the US JGOFS Bermuda Atlantic Time-series Study (BATS) site. Deep-Sea Research 43, 347–383.

Bates, N.R., Takahashi, T., Chipman, D.W., Knap, A.H., 1998. Variability of pCO_2 on diel to seasonal timescales in the Sargasso Sea near Bermuda. Journal of Geophysical Research 103, 15567–15585.

Bishop, J.K., Rossow, W.B., 1991. Spatial and temporal variability of global surface solar irradiance. Journal of Geophysical Research 96, 16398–16858.

Brewer, P.G., Goldman, J.C., 1976. Alkalinity changes generated by phytoplankton growth. Limnology and Oceanography 21, 108–117.

Bronk, D.A., Glibert, P.M., Ward, B.B., 1994. Nitrogen uptake, dissolved organic nitrogen release, and new production. Science 265, 1843–1846.

Buesseler, K.O., 1992. Do upper-ocean sediment traps provide an accurate record of particle flux? Nature 353, 420–423.

Cambella, A.D., Antia, N.J., Harrison, P.J., 1984. The utilization of inorganic and organic phosphorus compounds as nutrients by eukaryotic microalgae: a multidisciplinary perspective. Part 1. CRC Critical Reviews in Microbiology 10, 317–391.

Capone, D.G., Carpenter, 1982. Nitrogen fixation in the marine environment. Science, 217, 1140–1142.

Capone, D.G., Ferrier, M.D., Carpenter, E.J., 1994. Amino acid cycling in colonies of the planktonic marine cyanobacterium. *Trichodesmium thiebautii*. Applied and Environmental Microbiology 60, 3989–3995.

Capone, D.G., Zehr, J.P., Pearl, H.W., Bergman, B., Carpenter, E.J., 1997. *Trichodesmium*, a globally significant marine cyanobacterium. Science 276, 1221–1229.

Carlson, C.A., Ducklow, H.W., 1996. Growth of bacterioplankton and consumption of dissolved organic carbon in the Sargasso Sea. Aquatic Microbial Ecology 10, 69–85.

Carlson, C.A., Ducklow, H.W., Michaels, A.F., 1994. Annual flux of dissolved organic carbon from the euphotic zone in the northwestern Sargasso Sea. Nature 371, 405–408.

Carpenter, E.J., 1983. Physiology and ecology of marine planktonic *Oscillatoria (Trichodesmium)*. Marine Biology Letters 4, 69–85.

Carpenter, E.J., Capone, D.G., 1992. Nitrogen fixation in *Trichodesmium* blooms. In: Carpenter, E.J., Capone, D.G., Reuter, J.G. (Eds.), Marine Pelagic Cyanobacteria: *Trichodesmium* and other Diazotrophs. Kluwer Academic Publishers, Boston, pp. 211–217.

Carpenter, E.J., Capone, D.G., 1997. Biogeochemical tracers of the marine cyanobacterium *Trichodesmium*. Deep-Sea Research 44, 27–38.

Carpenter, E.J., McCarthy, J.J., 1975. Nitrogen fixation and uptake of combined nitrogenous nutrients by *Oscillatoria (Trichodesmium) thiebautii* in the western Sargasso Sea. Limnology and Oceanography 20, 389–401.

Carpenter, E.J., O'Neil, J.M., Dawson, R., Capone, D.G., Siddiqui, P.J.A., Roenneberg, T., Bergman, B., 1993. The tropical diazotrophic phytoplankter *Trichodesmium*: biological characteristics of two common species. Marine Ecology Progress Series 95, 295–304.

Carpenter, E.J., Price, C., 1977. Nitrogen fixation, distribution, and production of *Oscillatoria (Trichodesmium)* spp. in the western Sargasso and Caribbean Seas. Limnology and Oceanography 22, 60–72.

Carpenter, E.J., Romans, K., 1991. Major role of the cyanobacterium *Trichodesmium* in nutrient cycling in the North Atlantic Ocean. Science 254, 1356–1358.

Codispoti, L.A., 1989. Phosphorous vs. nitrogen limitation of new and export production. In: Berger, W.H., Smetacek, V.S., Wefer, G. (Eds.), Productivity of the Ocean: Present and Past. Wiley, New York, pp. 377–394.

del Giorgio, P.A., Cole, J.J., 1998. Bacterial growth efficiency in natural aquatic systems. Annual Review of Ecological Systems 29, 503–541.

Devassy, V.P., Bhattathiri, P.M.A., Quasim, S.Z., 1978. *Trichodesmium* phenomenon. Indian Journal of Marine Science 7, 168–186.

Dickson, A.G., Millero, F.J., 1987. A comparison of the equilibrium constants for the dissociation of carbonic acid in seawater. Deep-Sea Research 34, 1733–1743.

Dobson, F.W., Smith, S.D., 1988. Bulk models of solar radiation at sea. Quarterly Journal of the Royal Meteorological Society 144, 165–182.

Doney, S.C., 1996. A synoptic atmospheric surface forcing data set and physical upper ocean model for the US JGOFS Bermuda Atlantic Time-Series Study site. Journal of Geophysical Research 101, 25615–25634.

Eppley, R.W., 1972. Temperature and phytoplankton growth in the sea. Fisheries Bulletin 70, 1063–1085.

Falkowski, P.G., 1997. Evolution of the nitrogen cycle and its influence on the biological sequestration of CO_2 in the ocean. Nature 387, 272–275.

Fasham, J.J.R., Ducklow, H.W., McKelvie, S.M., 1990. A nitrogen-based model of plankton dynamics in the oceanic mixed layer. Journal of Marine Research 48, 591–639.

Fung, I.Y., Harrison, D.E., Lacis, A.A., 1984. On the variability of the net longwave radiation at the ocean surface. Reviews of Geophysics and Space Physics 22, 177–193.

Gruber, N., Keeling, C.D., Stocker, T.F., 1998. Carbon-13 constraints on the seasonal inorganic carbon budget at the BATS site in the northwestern Sargasso Sea. Deep-Sea Research 45, 673–717.

Gruber, N., Sarmiento, J.L., 1997. Global patterns in marine nitrogen fixation and denitrification. Global Biogeochemical Cycles 11, 235–266.

Glibert, P.M., Bronk, D.A., 1994. Release of dissolved organic nitrogen by marine diazotrophic cyanobacteria. *Trichodesmium* spp. Applied and Environmental microbiology 60, 3996–4000.

Halpert, M.S., Bell, G.D., 1997. Climate assessment for 1996. Bulletin of the American Meteorological Society 78, S1–S49.

Hansell, D.A., Carlson, C.A., 2001. Biogeochemistry of total organic carbon and nitrogen in the Sargasso Sea: control by convective overturn. Deep-Sea Research II 48, 1649–1667.

Hansell, D.A., Feely, R.A. Atmospheric intertropical convergences impact surface ocean carbon and nitrogen biogeochemistry in the tropical Pacific Ocean. Geophysical Research Letters, submitted for publication.

Hansson, I., 1973. A new set of acidity constants for carbonic acid and boric acid in seawater. Deep-Sea Research 36, 1635–1654.

Heinbokel, J.F., 1978. Studies on the functional role of tintinnids in the Southern California Bight. I. Grazing and growth rates in laboratory cultures. Marine Biology 47, 177–189.

Hood, R.R., Michaels, A.F., Capone, D.G., 2000. Answers sought to the enigma of marine nitrogen fixation. EOS 81, 138–139.

Hurrel, J.W., 1995. Decadal trends in the North Atlantic Oscillation: regional temperatures and precipitation. Science 269, 676–679.

Jenkins, W.J., 1988. Nitrate flux into the euphotic zone near Bermuda. Nature 331, 521–523.

Karl, D.M., Letelier, R., Hebel, D.V., Bird, D.F., Winn, C.D., 1992. *Trichodesmium* blooms and new nitrogen in the North Pacific gyre. In: Carpenter, E.J., Capone, D.G., Reuter, J.G. (Eds.), Marine Pelagic Cyanobacteria: *Trichodesmium* and other Diazotrophs. Kluwer Academic Publishers, Boston, pp. 219–237.

Karl, D.M., Letelier, R., Hebel, D., Tupas, L., Dore, J., Christian, J., Winn, C., 1995. Ecosystem changes in the North Pacific subtropical gyre attributed to the 1991–92 El Nino. Nature 373, 230–234.

Karl, D., Letelier, R., Tupas, L., Dore, J., Christian, J., Hebel, D., 1997. The role of nitrogen fixation in biogeochemical cycling in the subtropical North Pacific Ocean. Nature 388, 533–538.

Kirk, J.T.O., 1994. Light and Photosynthesis in Aquatic Ecosystems, 2nd Edition. Cambridge University Press, Cambridge, UK, 509pp.

Knap, A.H., Michaels, A.F., Dow, R.L., Johnson, R.J., Gundersen, K., Sorensen, J.C., Close, A.R., Howse, F.A., Hammer, M., Bates, N., Doyle, A., Waterhouse, T., 1993. BATS Methods Manual, Version 3. US JGOFS Planning Office, Woods Hole, MA.

Large, W.G., Pond, S., 1982. Sensible and latent heat flux measurements over the ocean. Journal of Physical Oceanography 12, 464–482.

Ledwell, J.R., Watson, A.J., Law, C.S., 1998. Mixing of a tracer in the pycnocline. Journal of Geophysical Research 103, 21,499–21,529.

Letelier, R., 1994. Studies on the ecology of *Trichodesmium* spp. (Cyanophyceae) in the Central North Pacific Gyre. Ph.D. Thesis, University of Hawaii.

Letelier, R.M., Karl, D.M., 1996. Role of *Trichodesmium* spp. in the productivity of the subtropical North Pacific Ocean. Marine Ecology Progress Series 133, 263–273.

Letelier, R.M., Karl, D.M., 1998. *Trichodesmium* spp. physiology and nutrient fluxes in the North Pacific subtropical gyre. Aquatic Microbial Ecology 15, 265–276.

Lipschultz, F., Owens, N.J.P., 1996. An assessment of nitrogen fixation as a source of nitrogen to the North Atlantic Ocean. Biogeochemistry 35, 261–274.

Mague, T.H., Mague, F.C., Holm-Hansen, O., 1977. Physiology and chemical composition of nitrogen-fixing phytoplankton in the central North Pacific Ocean. Marine Biology 41, 213–227.

Maloney, C.L., Field, J.G., 1991. The size-based dynamics of plankton food webs. I. A simulation model of carbon and nitrogen flows. Journal of Plankton Research 13, 1003–1038.

Marchal, O., Monfray, P., Bates, N.R., 1996. Spring-summer imbalance in dissolved inorganic carbon in the mixed layer of the Northwestern Sargasso Sea. Tellus 48, 115–134.

McCreary J.P., Jr., Kohler, K.E., Hood, R.R., Olson, D.B., 1996. A four-component ecosystem model of biological activity in the Arabian Sea. Progress in Oceanography 37, 193–240.

McGillicuddy, D.J., Robinson, A.R., 1997. Eddy induced nutrient supply and new production in the Sargasso Sea. Deep-Sea Research 44, 1427–1499.

McGillicuddy, D.J., Robinson, A.R., Siegel, D.A., Jannasch, H.W., Johnson, R.J., Dickey, T.D., McNeil, J., Michaels, A.F., Knap, A.H., 1998. Influence of mesoscale eddies on new production in the Sargasso Sea. Nature 394, 263–266.

Mehrbach, C., Culberson, C.H., Hawley, J.E., Pytkowicz, R.M., 1973. Measurement of the apparent dissociation constants of carbonic acid in seawater at atmospheric pressure. Limnology and Oceanography 18, 897–907.

Michaels, A.F., Bates, N.R., Buesseler, K.O., Carlson, C.A., Knap, A.H., 1994. Carbon-cycle imbalances in the Sargasso Sea. Nature 372, 537–540.

Michaels, A.F., Knap, A.H., 1996. Overview of the US JGOFS Bermuda Atlantic Time-series Study and the Hydrostation S program. Deep-Sea Research 43, 157–198.

Michaels, A.F., Olson, D., Sarmiento, J.L., Ammerman, J.W., Fanning, K., Jahnke, R., Knap, A.H., Lipschultz, F., Prospero, J.M., 1996. Inputs, losses and transformations of nitrogen and phosphorous in the pelagic North Atlantic Ocean. Biogeochemistry 35, 181–226.

Millero, F.J., 1979. The thermodynamics of the carbonate system in seawater. Geochimica et Cosmochimica Acta 43, 1651–1661.

Montoya, J.P., Carpenter, E.J., Capone, D.G., Diazotroph control of nitrogen isotope abundances in the oligotrophic Ocean. Deep-Sea Research, submitted for publication.

Mulholland, M.R., Capone, D.G., 1999. Nitrogen fixation, uptake and metabolism in natural and cultured populations of *Trichodesmium* spp. Marine Ecology Progress Series 188, 33–49.

O'Neil, J.M., Roman, M.R., 1994. Ingestion of the cyanobacterium *Trichodesmium* spp. by pelagic harpacticoid copepods Macrosetella, Miracia, and Oculosetella. Hydrobiologia 292/293, 235–240.

Orcutt, K.M., Lipschultz, F.J., Gundersen, K., Arimoto, R., Michaels, A.F., Knap, A.H., Gallon, J.R., 2001. A seasonal study of the significance of N_2 fixation by *Trichodesmium* at the Bermuda Atlantic Time-series (BATS) site. Deep-Sea Research II 48, 1583–1608.

Parsons, T.R., Takahashi, M., Hargrave, B., 1984. Biological Oceanographic Processes. Pergamon Press, Ontario, Canada, 330pp.

Platt, T., Gallegos, C.L., Harrison, W.G., 1980. Photoinhibition of photosynthesis in natural assemblages of marine phytoplankton. Journal of Marine Research 38, 687–701.

Press, W.H., Teukolsky, S.A., Vetterling, W.T., Flannery, B.P., 1992. Numerical Recipes in FORTRAN: the Art of Scientific Computing, 2nd Edition. Cambridge University Press, Cambridge, New York.

Price, J.F., Weller, R.A., Pinkel, R., 1986. Diurnal cycling: observations and models of the upper ocean response to diurnal heating, cooling, and wind mixing. Journal of Geophysical Research 91, 8411–8427.

Redfield, A.C., Ketchum, B.H., Richards, F.A., 1963. The influence of organisms on the composition of sea-water. In: Hill, M.N. (Ed.), The Sea, Vol. 2. Interscience Publications, New York, pp. 26–77.

Romans, K.M., Carpenter, E.J., 1994. Buoyancy regulation in the colonial diazotrophic cyanobacterium *Trichodesmium tenue:* ultrastructure and storage of carbohydrate, polyphosphate and nitrogen. Journal of Phycology 30, 935–942.

Sambrotto, R.N., Savidge, G., Robinson, C., Boyd, P., Takahashi, T., Karl, D.M., Langdon, C., Chipman, D., Marra, J., Codispoti, L., 1993. Elevated consumption of carbon relative to nitrogen in the surface ocean. Nature 363, 248–250.

Sarmiento, J.L., Armstrong, R.A., 1997. US JGOFS Synthesis and Modeling Project Implementation Plan. The Role of Oceanic Processes in the Global Carbon Cycle. AOS Program, Princeton University Press, Princeton, NJ, P.O. Box CN710.

Sharp, J.H., 1983. The distributions of inorganic nitrogen and dissolved and particulate organic nitrogen in the sea. In: Carpenter, E.J., Capone, D.G. (Eds.), Nitrogen in the Marine Environment. Academic Press Inc, New York, pp. 1–35.

Siegel, D.A., McGillicuddy, D.J., Fields, E.A., 1999. Mesoscale eddies, satellite altimetry and new production in the Sargasso Sea. Journal of Geophysical Research 104, 13359–13379.

Smolarkiewicz, P.K., 1983. A simple positive definite advection scheme with small implicit diffusion. Monthly Weather Review 111, 479–486.

Tans, P.P., Fung, I.Y., Takahashi, T., 1990. Observational constraints on the global atmospheric CO_2 budget. Science 247, 1431–1438.

Tyrrell, T., 1999. The relative influences of nitrogen and phosphorus on oceanic primary production. Nature 400, 525–531.

UNESCO, 1987. Thermodynamics of the carbon dioxide system in seawater. Technical Papers in Marine Science, 51, UNESCO, Paris, France.

Verity, P.G., 1985. Grazing, respiration, excretion and growth rates of tintinnids. Limnology and Oceanography 30, 1268–1282.

Vidal, M., Duarte, C.M., Agusti, S., 1999. Dissolved organic nitrogen and phosphorous pools and fluxes in the central Atlantic Ocean. Limnology and Oceanography 44, 106–115.

Villareal, T.A., Carpenter, E.J., 1990. Diel buoyancy regulation in the marine diazotrophic cyanobacterium *Trichodesmium thiebautii*. Limnology and Oceanography 35, 1832–1837.

Walsby, A.E., 1992. The gas vesicles and buoyancy of *Trichodesmium*. In: Carpenter, E.J., Rueter, D.G. (Eds.), Marine Pelagic Cyanobacteria: *Trichodesmium* and other Diazotrophs. Kluwer, Dordrecht, pp. 141–161.

Wanninkhof, R., 1992. Relationship between wind speed and gas exchange over the ocean. Journal of Geophysical Research 97, 7373–7382.

Weiss, R., 1974. Carbon dioxide in water and seawater — the solubility of a non-ideal gas. Marine Chemistry 2, 203–215.

Wheeler, P.A., Kirchman, D.L., 1986. Utilization of inorganic and organic nitrogen by bacteria in marine systems. Limnology and Oceanography 31, 998–1009.